1 Comparative anatomy of the carotid canal in the Miocene small-bodied catarrhine *Pliobates*

2 *cataloniae*

3

4 **Abstract**

5 The small-bodied Miocene catarrhine *Pliobates cataloniae* (11.6 Ma, Spain) displays a

6 mosaic of catarrhine symplesiomorphies and hominoid synapomorphies that hinders

7 deciphering its phylogenetic relationships. Based on cladistic analyses it has been

8 interpreted as a stem hominoid or as a pliopithecoid. Intriguingly, the carotid canal

9 orientation of *Pliobates* was originally described as hylobatid-like. The variation in carotid

10 canal morphology among anthropoid clades shown in previous studies suggests that this

11 structure might be phylogenetically informative. However, its potential for phylogenetic

12 reconstruction among extinct catarrhines remains largely unexplored. Here we quantify the

13 orientation, proportions, and course of the carotid canal in *Pliobates*, extant anthropoids

14 and other Miocene catarrhines (*Epipliopithecus*, *Victoriapithecus*, and *Ekembo*) using 3D

15 morphometric techniques. We also compute phylogenetic signal and reconstruct the

16 ancestral carotid canal course for main anthropoid clades. Our results reveal that carotid

17 canal morphology embeds strong phylogenetic signal but mostly discriminates between

18 platyrrhines and catarrhines, with an extensive overlap among extant catarrhine families.

19 The analyzed extinct taxa display a quite similar carotid canal morphology more closely

20 resembling that of extant catarrhines. Nevertheless, our results for *Pliobates* highlight some

21 differences compared with the pliopithecid *Epipliopithecus*, which displays a somewhat

22 more platyrrhine-like morphology. In contrast, *Pliobates* appears as derived toward the

23 modern catarrhine condition as the stem cercopithecid *Victoriapithecus* and the stem

24 hominoid *Ekembo*, which more closely resemble one another. Moreover, *Pliobates* appears

somewhat derived toward the reconstructed ancestral hominoid morphotype, being more similar than other Miocene catarrhines to the condition of great apes and the hylobatid *Symphalangus*. Overall, our results rule out previously noted similarities in carotid canal morphology between *Pliobates* and hylobatids, but do not show particular similarities with pliopithecoids either—as opposed to extant and other extinct catarrhines. Additional analyses will be required to clarify the phylogenetic relationships of *Pliobates*, particularly given its dental similarities with dendropithecids.

Keywords: Internal carotid artery; Petrosal; Geometric morphometrics; Fossil primates; Phylogeny; Evolution.

1. Introduction

1.1. Pliobates *and catarrhine evolution*

Crown catarrhines include two main extant clades distinguished at the superfamily rank: Old World monkeys (Cercopithecoidea) and apes and humans (Hominoidea). Earliest stem catarrhines have been reported from the latest Eocene (34.5–29.5 Ma) of Afro-Arabia (Seiffert, 2006, 2012; Seiffert et al., 2010). In turn, earliest crown catarrhines (both cercopithecoids and hominoids) date back to the late Oligocene (~25 Ma) of East Africa (Stevens et al., 2013)—in accordance with molecular estimates indicating that the cercopithecoid–hominoid divergence occurred during the Oligocene (Chatterjee et al., 2009; Perelman et al., 2011; Springer et al., 2012; Finstermeier et al., 2013; Pozzi et al., 2014). Catarrhines did not disperse into Eurasia until later in the early Miocene, following the closure of the Tethys Seaway and the establishment of intermittent land bridges at ~19 Ma (Harzhauser et al., 2007; Harrison, 2013). Several catarrhine lineages eventually dispersed

49 from Afro-Arabia into Eurasia (Roos et al., 2019; Gilbert et al., 2020a), including:

50 pliopithecoids (considered an Eurasian clade of stem catarrhines, first recorded ~18–17 Ma;

51 Harrison and Gu, 1999; Begun, 2002, 2017; Harrison, 2013); hylobatids (first recorded ~13.8–

52 12.5 Ma; Gilbert et al., 2020b); large-bodied hominoids (presumably hominids, first recorded

53 ~16.5–14 Ma; Casanovas-Vilar et al., 2011; Harrison, 2017); and various lineages of

54 cercopithecoid primates, successively recorded at different times in Eurasia, namely

55 colobines (~8.5 Ma; Alba et al., 2015a), cercopithecins (~8–6.5 Ma; Gilbert et al., 2014),

56 macaques (~5.9–5.3 Ma; Alba et al., 2014a), and geladas (1.6–1.2 Ma; Alba et al., 2014b).

57 A panoply of small-bodied, putative stem catarrhine genera (including, but not restricted

58 to, dendropithecids) are recorded in the early to middle Miocene of Africa (Harrison, 2010,

59 2013). Some Miocene Eurasian taxa have previously been linked to some of these African

60 stem catarrhines—implying yet another catarrhine dispersal event from Africa—but such

61 claims have been mostly rejected by reinterpreting them as pliopithecoids or hylobatids

62 (Harrison, 2016 and references therein). The most likely exception is some isolated dental

63 remains from Pakistan (~17–16 Ma; Barry et al., 1987; Bernor et al., 1988), which are most

64 similar to African dendropithecids (Harrison, 2016) but might ultimately prove to be stem

65 pliopithecoids (Sankhyan et al., 2017). In turn, as remarked by Roos et al. (2019), the small-

66 bodied catarrhine *Pliobates* (middle/late Miocene of Spain, 11.6 Ma; Alba et al., 2015b)

67 might denote an additional out-of-Africa dispersal event of catarrhines unless it is

68 interpreted as a pliopithecoid. This taxon was originally recovered by Alba et al.'s (2015b)

69 cladistic analysis as a stem hominoid morphologically more derived than *Proconsul* s.l.

70 (currently split into *Proconsul* s.s. and *Ekembo*; McNulty et al., 2015) and subsequently

71 reinterpreted as a pliopithecoid by different cladistic analyses (Nengo et al., 2017; Gilbert et

72 al., 2020b), as first suggested by Benefit and McCrossin (2015). However, given the mosaic

73   nature of its cranial and postcranial skeleton—combining plesiomorphic, stem catarrhine-

74   like features (including dental resemblances with dendropithecids) with crown hominoid

75   synapomorphies (Alba et al., 2015b)—the possibility remains that *Pliobates* is a late

76   descendant of an African stem catarrhine lineage.

77   Deciphering the phylogenetic position of *Pliobates* would have important implications for

78   our current understanding of catarrhine evolution and paleobiogeography during the

79   Miocene. If ultimately shown to be a pliopithecoid or as a member of a different stem

80   catarrhine lineage, it would imply remarkable cranial and postcranial convergences with

81   crown hominoids; in turn, if interpreted as a non-pliopithecoid stem catarrhine or as a stem

82   hominoid, it would indicate that pliopithecoids were not the only small catarrhines to

83   disperse from Africa into Europe. Unfortunately, determining the evolutionary history and

84   phylogenetic relationships of small-bodied catarrhines is still hindered by the fragmentary

85   nature of their fossil remains and the incompleteness of their fossil record—with long ghost

86   lineages for both pliopithecoids and hylobatids. Deciphering the phylogenetic position of

87   extinct taxa ultimately requires performing cladistic analyses with all available evidence from

88   multiple anatomical regions. However, as mentioned above, previous attempts in this regard

89   have yielded contradictory results for *Pliobates* (compare Alba et al., 2015b with Nengo et

90   al., 2017 and Gilbert et al., 2020b). Therefore, additional research on the various characters

91   included in these analyses is required to refine their definition and scoring for both extant

92   and extinct taxa. With this aim in mind, here we focus on one of the most intriguing features

93   included in the original diagnosis of *Pliobates*: the orientation of the carotid canal, which was

94   originally described as most closely resembling hylobatids than either pliopithecoids or other

95   hominoids (Alba et al., 2015b). Given the potential implications of such similarities—if

96   interpreted as a hylobatid synapomorphy or hominoid symplesiomorphy—we decided to

4

97   analyze them quantitatively by means of a novel morphometric approach devised to

98   measure the size and shape of the carotid canal. To the best of our knowledge, this is the

99   first study to quantitatively assess the orientation, proportions, and course of this

100   anatomical structure in extant and extinct anthropoids.

101

102   *1.2. The carotid canal in primate phylogenetics*

103   All haplorrhines and non-cheirogaleid lemuriforms have an internal carotid artery

104   enclosed by a bony canal (termed 'carotid canal') that derives from the anterior lamina of

105   the petrosal plate (Bugge, 1974, 1980; Cartmill et al., 1981; MacPhee and Cartmill, 1986; Kay

106   et al., 2008; Boyer et al., 2016). The carotid canal runs from the posterolaterally located

107   external carotid foramen to the endocranial space (Bugge, 1980; MacPhee and Cartmill,

108   1986; Kay et al., 2008; Boyer et al., 2016). In haplorrhines, the carotid canal displays a

109   'perbullar pathway': it is located in the primary medial wall of the auditory bulla and runs

110   through the middle ear cavity, passing through the transverse septum that separates the

111   tympanic cavity from the anterior accessory cavity (Cartmill et al., 1981; MacPhee and

112   Cartmill 1986; Kay et al., 2008). The canal then opens more anteromedially into the

113   endocranial surface, with an opening located either on the basisphenoid or between the

114   basisphenoid and petrosal (Boyer et al., 2016). In adult anthropoids, one of the two

115   branches of the internal carotid artery (the stapedial artery) is missing and only the

116   promontory artery remains patent (Bugge 1974, 1980; Rosenberger and Szalay, 1980;

117   MacPhee and Cartmill, 1986; Kay et al., 2008; Boyer et al., 2016). Therefore, the carotid

118   canal of anthropoid primates corresponds to a unique and well-developed bony enclosure.

119   Low homoplasy is one of the most important criteria for choosing phylogenetically

120   informative morphological characters (Lieberman, 1999). Among characters least affected by

121 homoplasy (convergence, parallelism, reversal, and homoiology), soft-tissue traits have

122 previously been proven more efficient in producing accurate primate phylogenies than hard-

123 tissue traits (Gibbs et al., 2000, 2002; Diogo and Wood, 2011). Given that vessel and nerve-

124 related characters are soft-tissue traits, this rationale might potentially apply to the carotid

125 canal as well. A few previous studies have included carotid canal features in character-taxon

126 matrices devised for cladistic analysis, focusing on the position of the carotid foramen in the

127 bulla as well as on the overall direction and orientation of the canal itself (Beard and

128 MacPhee, 1994; Ross, 1994; Shoshani et al., 1996; Ross et al., 1998; Kay et al., 2008; Alba et

129 al., 2015b). These studies aimed at resolving phylogenetic relationships among higher-rank

130 primate clades (Beard and MacPhee, 1994; Ross, 1994; Shoshani et al., 1996; Ross et al.,

131 1998; Kay et al., 2008) and/or deciphering the phylogenetic relationships of particular fossil

132 taxa (Ross et al., 1998; Kay et al., 2008; Alba et al., 2015b). Nonetheless, some of them found

133 differences between platyrrhines and catarrhines, as well as among some catarrhine groups.

134 Based on these studies, the morphology of the carotid canal seems promising for

135 phylogenetic reconstruction in catarrhine primates. However, the exact phylogenetic

136 potential of this structure for distinguishing among catarrhine subclades and, hence,

137 clarifying the relationships of extinct taxa remains unexplored.

138   In the light of all the considerations above, the aim of this paper is threefold: (1)

139 investigate the orientation, proportions, and course of the carotid canal in a wide sample of

140 extant anthropoid primates, to test its potential for phylogenetic inference in extinct

141 catarrhines; (2) re-evaluate previously noted differences and similarities among several

142 catarrhine clades; and (3) describe the carotid canal morphology of *Pliobates* and compare it

143 with that of extant and fossil catarrhines, so as to gain additional insight on the controversial

144 phylogenetic relationships of this genus. To do so, we collected μCT scans of both fossil taxa

145 and an extant comparative sample, and developed a newly devised semiautomatic iterative

146 protocol to obtain comparable 3D carotid canal surfaces (i.e., 3D models). These are

147 analyzed by means of traditional morphometrics and three-dimensional geometric

148 morphometric (3DGM) and imaging techniques, to quantify the orientation, proportions,

149 and course of the carotid canal within the petrosal in a standardized manner.

150

151 **2. Materials and methods**

152 *2.1. Materials*

153 <u>Studied sample</u> This study focuses on the cranium of the holotype (IPS58443) of *Pliobates*

154 *cataloniae*, which consists of a partial skeleton (Alba et al., 2015b). The carotid canal is

155 entirely preserved in the right temporal fragment (IPS58443.1; Alba et al., 2015b: Fig. 1A). In

156 contrast, in the left temporal fragment (same specimen) the inferiormost part of the canal is

157 broken, with most of its lateral and anterior walls missing along a length of >1.5 mm.

158 IPS58443.1 was originally scanned at a resolution of 95 μm (Alba et al., 2015b). To explore

159 fine bony structures, the specimen was scanned again by X-ray microtomography at the

160 Centro Nacional de Investigación sobre la Evolución Humana (CENIEH, Burgos, Spain) using a

161 Phoenix V|Tome|X s240 μCT scanner with the following parameters: 0.35 mA current, 170

162 kV voltage, 0.2 mm Cu filter, and a magnification of 9.52. The final reconstructed volume has

163 an isometric voxel size of 21 μm.

164 <u>Fossil comparative sample</u> Three Miocene catarrhines are included in the comparative

165 sample: the Miocene pliopithecoid *Epipliopithecus vindobonensis* (see Zapfe, 1961), the stem

166 cercopithecoid (victoriapithecid) *Victoriapithecus macinnesi* (see review in Benefit and

167 McCrossin, 1997), and the stem hominoid (proconsulid) *Ekembo heseloni* (see review in

168 McNulty et al., 2015). There are four available fragmentary temporal bones of

169   *Epipliopithecus* (Zapfe, 1961): NMB OE 303 (right and left temporals, individual II), NHMW

170   1970/1397/0002 (right temporal, individual III; holotype), and NHMW 1970/1397/0003 (left

171   temporal, individual III; holotype). The carotid canal is only sufficiently preserved in the

172   latter specimen, which includes a portion of the bulla, the external acoustic meatus, and

173   most of the petrosal (Zapfe, 1961: Fig. 28). In contrast, the anterior end of the canal is

174   missing from the remaining specimens. The petrosal of the holotype was scanned at the

175   Vienna µCT lab (Vµ-CTL) using a Viscom X8060 µCT scanner with the following parameters:

176   0.24 mA current, 120 kV voltage, 0.5 mm Cu filter, and a magnification of 7.50. The final

177   reconstructed volume has an isometric voxel size of 22 µm. *Ekembo heseloni* is represented

178   by the right temporal specimen KNM-RU 2036al (Davis and Napier, 1963: Fig. 1; Alba et al.,

179   2015b: Fig. 4C), which is part of the holotype (Walker et al., 1993), while *V. macinnesi* is

180   represented by the left temporal of the cranium KNM-MB 29100 (Benefit and McCrossin,

181   1997: Fig. 1; Benefit, 1999: Fig. 3; Jablonski and Frost, 2010: Fig. 23.1). The µCT scans of

182   KNM-RU 2036al and KNM-MB 29100 have isometric voxel sizes of 64 µm and 44 µm,

183   respectively. They were both kindly made available for this study by the Department of Earth

184   Sciences, National Museums of Kenya (which holds the copyright) and the Department of

185   Human Evolution, Max Plank Institute for Evolutionary Anthropology, Leipzig, Germany.

186   <u>Extant comparative sample</u> Our extant comparative sample consists of µCT scans of 127

187   crania belonging to 41 anthropoid species (13 platyrrhines and 28 catarrhines) from 36

188   genera, representing all extant hominoid genera as well as all cercopithecoid subtribes and

189   platyrrhine (sub)families (Table 1; Supplementary Online Material [SOM] Table S1). A

190   minimum of three individuals per genus are included. Ontogenetic changes in basicranial

191   angulation and elongation—somewhat related to each other and potentially affecting

192   petrosal morphology—continue up to adulthood as measured by M^3 eruption (Lieberman

193   and McCarthy, 1999; Lieberman et al., 2000). Therefore, all individuals included in the

194   comparative sample are fully adult (exhibiting the M^3 in occlusion, or the M^2 in

195   callitrichines). Most of the μCT scans included in our extant comparative sample were

196   downloaded from MorphoSource (https://www.morphosource.org; Table 1; SOM Table S1).

197   Three μCT scans of specimens from the AMNH were kindly provided by Sergio Almécija,

198   while seven additional μCT scans of specimens housed in the Institut Català de Paleontologia

199   Miquel Crusafont (Sabadell, Spain) were scanned at the CENIEH. The μCT resolution for the

200   specimens included in the extant comparative sample ranges from 27 to 131 μm (Table 1;

201   SOM Table S1).

202

203   *2.2. Morphometric methods*

204   <u>Segmentation</u> For each specimen, the carotid canal was virtually extracted through

205   semiautomatic threshold-based segmentation in Avizo v. 7.0 (Visualization Sciences Group,

206   Mérignac). The right carotid canal was segmented for most specimens; when this was not

207   possible, the left canal was segmented and mirrored. Both extremities of the resulting 3D

208   canal surfaces (i.e., 3D models) were cut along homologous planes to allow their comparison

209   among different individuals. First, to cut the posterior end of the canal, we used a best-fit

210   plane based on landmarks placed on its external aperture (Fig. 1a, I; SOM Fig. S1a, b). Then,

211   the anterior limit of the carotid canal was identified by determining a landmark on the

212   anterior part of the petrosal (the 'intersection ridge–groove' [IRG]; Fig. 1b–I; SOM Fig. S1c, d;

213   see SOM S1) and cut through such a homologous point using a script coded in R v. 4.0.2 (R

214   Core Team, 2020; see SOM file S1).

215   <u>Alignment and canal orientation</u> The orientation of the carotid canal within the petrosal was

216   quantified by means of two 2D angles representing the canal superior orientation along the

217   (para)sagittal plane (2DYZA) and its medial orientation along a transverse plane (2DXYA)—

218   which can be related to canal 'orientation' and 'direction' sensu Alba et al. (2015b: Tables S5

219   and S6), respectively. Each was computed as the angle between the vector connecting the

220   canal endpoints (from posterior to anterior) and a standard reference vector. Both the canal

221   vector and the reference vector were computed after performing a Procrustes alignment

222   based on petrosal/tympanic landmarks (Fig. 2; Table 2) and applying the translation-scaling-

223   rotation parameters resulting from this alignment to the two canal endpoints (SOM S1). This

224   procedure allowed us to retain the information on the position, orientation and shape

225   variation of the canal inside the petrosal. For both angles, the standard reference vector

226   corresponds to a 2D vector parallel to the anteroposterior cranial axis (from posterior to

227   anterior), in lateral view for 2DYZA and in superior view for 2DXYA (Fig. 3). Aligning the

228   carotid canal on the basis of petrosal/tympanic landmarks instead of the cranium as a whole

229   enables the analysis of fragmentary fossils and has several advantages (see SOM S1 for

230   further details), while being consistent with previous studies (Beard and MacPhee, 1994;

231   Ross, 1994; Shoshani et al., 1996; Ross et al., 1998; Kay et al., 2008; Alba et al., 2015b) that

232   assessed carotid foramen locations relative to the bulla instead of general cranial axes or

233   planes.

234   <u>Volume and length</u> The volume (V, in mm^3) of the 3D canal surfaces was computed using the

235   module 'Surface Area Volume' in Avizo. To calculate canal length (L, in mm), we used

236   equidistant slices between the two canal endpoints (which correspond to type III landmarks;

237   Bookstein, 1991). These slices were used to generate 8 additional equidistant semilandmarks

238   that follow the canal streamline using the 'digit.curve' function of 'Geomorph' v. 3.3.1

239   (Adams et al., 2019), summing a total of 10 canal landmarks, which define the canal

240   streamline. This canal landmark configuration thus corresponds to a total of 10 canal

241   streampoints. Canal length was taken as the sum of the length of the resulting nine canal

242   segments (see SOM S1 for further details).

243   Robusticity index Carotid canal proportions were measured by a dimensionless index of

244   canal robusticity as $L/V^{1/3}$. Even though the carotid canal is a hollow structure, we refer to

245   this index as 'robusticity' because it measures how thick the canal is on average relative to

246   its length. Low values of the index denote robust canals, whereas high values denote slender

247   canals. The same terms have been applied to other hollow cranial structures, such as the

248   semicircular canals of the bony labyrinth (Urciuoli et al., 2020, 2021a, 2021b). The diameter

249   (and hence the cross-sectional area) of the carotid canal varies along its length, so that using

250   the cube root of the volume as the denominator is equivalent to relying on the hypothetical

251   average cross-sectional area. We used the cube root of the volume to make the index

252   dimensionless (i.e., a shape variable), and verified that the robusticity index was free from

253   allometric (size-scaling) effects by computing a phylogenetic generalized least-squares

254   (PGLS) regression of ln L against ln $V^{1/3}$ on the species means of the whole sample. We

255   further computed a major axis regression of the same parameters, using the function

256   'lmodel2' of the R package 'lmodel2' v. 1.7-3 (Legendre, 2018). The objective was to test

257   whether length and volume of the carotid canal covary in a linear (i.e., isometric) or non-

258   linear (i.e., allometric) fashion, and to do so under the assumptions that the independent

259   variable is measured with error (major axis) or without error (PGLS). Note that, under

260   geometric similarity, linear dimensions and volumes are expected to be correlated with an

261   allometric slope of 1/3 (Gould, 1966). However, this does not apply here because we used

262   the cube root of the canal volume, so that allometry would imply an allometric slope

263   significantly different from 1.

264   <u>Canal course configuration</u> To assess carotid canal course within the petrosal, we applied the

265   translation-scaling-rotation parameters resulting from the alignment of the

266   petrosal/tympanic landmarks described above to the 10 canal landmark configuration. As for

267   canal orientation, we were able to retain the position, orientation and shape variation of the

268   canal inside the petrosal. Therefore, the postalignment 10 canal landmark configuration

269   represents the course of the carotid canal within the petrosal (SOM S1) and will be

270   thereafter referred to as 'carotid canal course configuration'.

271   <u>Size scaling</u> To better understand the influence of size-scaling (allometric) effects on carotid

272   canal shape, we computed multiple bivariate regressions using PGLS. On the one hand, we

273   relied on allometric regressions of canal measurements (as measured by L and $V^{1/3}$) against

274   overall canal size (as measured by centroid size [CS]; see Section 2.3 below) and body size (as

275   measured by body mass [BM]); the allometric regression between CS and BM was also

276   computed. On the other hand, we computed regressions between carotid canal shape—

277   including not only the above-mentioned index of canal robusticity, but also the multivariate

278   shape variables derived by means of between-group principal component analysis (bgPCA;

279   see Section 2.3 below)—against log-transformed carotid canal size (as measured by $V^{1/3}$ and

280   CS) and BM. To minimize the effects of body size dimorphism, for each taxon we relied

281   exclusively on average female BM taken from the literature (Smith and Jungers, 1997;

282   Delson et al., 2000; Turner et al., 2018). Natural logarithms (ln) were used in all instances.

283   For allometric regressions between metrical linear variables, the null hypothesis of isometry

284   was rejected when unity was excluded from the 95% CI of the allometric slope. In contrast,

285   for bivariate regressions of shape vs. size, isometry was rejected when the regression was

286   significant (i.e., when the slope was significantly different from zero).

287

2.3. Between-group principal component analyses

Carotid canal course variation among clades was examined using a bgPCA of the carotid canal course configurations using the 'groupPCA' function of the R package 'Morpho' v. 2.8 (Schlager, 2017). We used the following four main crown anthropoid clades as grouping factor: platyrrhines, cercopithecids, hylobatids, and hominids, with fossils projected onto the morphospace a posteriori. The bgPCA analysis was repeated based on a catarrhine-only subsample to see if it provided a better discrimination among extant catarrhine families once the variance introduced by platyrrhines was removed.

As explained in the preceding section, allometric effects on canal course configuration were assessed by means of PGLS regressions of between-group principal component (bgPCs) against log-transformed canal size (ln CS and ln $V^{1/3}$) or log-transformed body size (ln BM)— see Section 2.2 for further details.

We verified that the bgPCA grouping structure was not spurious by comparing our bgPCA results with those of a cross-validated bgPCA (Cardini et al., 2019). This procedure iteratively resamples the data set by excluding one individual at a time and using the remaining ($n - 1$) individuals to compute the model that is then used to classify the omitted individual. A cross-validated bgPCA significantly reduces the distortion of mean group differences, so that its comparison with the non-cross-validated bgPCA allows one to ascertain whether (or to what extent) the latter is affected by spurious grouping effects. As further recommended by Cardini and Polly (2020), we also relied on a permutational analysis of variance (PERMANOVA) to (1) explore the significance (p) of group mean differences and (2) compute the variance (R^2) explained by them. The permutations consist in randomly resampling n times the data set (thus modifying group composition, as the individuals are permuted), each time recomputing the distance between the centroids of all pairs of newly formed

groups. Based on this set of permutations, here consisting of between-group Euclidean distances, both p and R^2 were computed within the full space of canal course configurations as well as within the bgPCA spaces (both standard and cross-validated bgPCs). As in the case of the cross-validated bgPCA scatterplot, comparing the p and R^2 values of the bgPCA (before and after cross-validation) with those of the raw canal course configuration coordinates permits verifying if the former inflates the differences among groups. These computations were done using the 'lm.rrpp' function of the R package 'RRPP' v. 0.6.1 (Collyer and Adams, 2018).

The discrimination among a priori defined groups was evaluated on the basis of correctly classified individuals after cross-validation. Posterior probabilities of group membership were computed for fossil specimens based on the squared Mahalanobis distances between their bgPC scores (bgPC1 and bgPC2) and those of extant group centroids using the 'typprobClass' function of 'Morpho'. Finally, a neighbor-joining (NJ) cluster was computed using a matrix of Euclidean distances based on the raw coordinates of the canal course configurations with the 'nj' function of the R package 'phangorn' v. 2.5.5 (Schliep, 2011).

2.4. Statistical analyses

Box and whisker plots were employed to assess the variation in carotid canal orientation (2DYZA and 2DXYA), proportions (index $L/V^{1/3}$), and course (bgPC1 and bgPC2). To test for significant differences among extant groups, we used Kruskal-Wallis non-parametric tests and Bonferroni-corrected Mann-Whitney post hoc pairwise comparisons performed in R. When significant differences were found, *Pliobates* and other extinct genera were compared with the distributions of extant groups using z-scores—computed as z = (individual value –

14

335 group mean) / SD—to assess if the fossil specimens fall within the variation of the latter ($|z|$

336 ≤ 1.96).

337

338 *2.5. Phylogenetically informed methods*

339 <u>Phylogenetic tree</u> To compute PGLS regressions and the phylomorphospaces, as well as to

340 quantify phylogenetic signal, we used a time-calibrated phylogenetic tree among the

341 investigated taxa. The tree for the extant taxa was primarily derived from the 10kTrees v.3

342 website (Arnold et al., 2010), although some species that were not included there were

343 added a posteriori following Meyer et al. (2011) and Springer et al. (2012)—see SOM S1 for

344 further details. Two different hypotheses for the extinct genera were considered, except for

345 *Victoriapithecus*, which was invariably considered a stem cercopithecoid. Under hypothesis 1

346 (SOM Fig. S2a), *Epipliopithecus, Ekembo*, and *Pliobates* were considered successive stem

347 hominoids, following the results of Alba et al.'s (2015b) cladistic analysis. In contrast, under

348 hypothesis 2 (SOM Fig. S2b), only *Ekembo* was considered a stem hominoid, while both

349 *Pliobates* and *Epipliopithecus* were considered stem catarrhines (pliopithecoids), following

350 the results of other cladistic analyses (Nengo et al., 2017; Gilbert et al., 2020b). The tip and

351 divergence dates for the extinct taxa are detailed in SOM S1.

352 <u>Phylogenetic signal</u> To assess the phylogenetic signal embedded in carotid canal course, we

353 computed Pagel's λ (Pagel, 1999) and Blomberg's K (Blomberg et al., 2003) statistics using

354 the R package 'phytools' v. 0.7-70 (Revell, 2012). These metrics compare the variance in the

355 phylogenetic tree tips relative to that expected under a Brownian motion evolutionary

356 model. Pagel's λ measures the covariance among related species and ranges from 0 (no

357 phylogenetic signal) to 1 (high phylogenetic signal). In turn, Blomberg's K reflects to what

358 extent the phylogenetic tree matches the variance in the data (and where variance is

359   concentrated): K ≈ 1 means that trait evolution approximates the expectations under a

360   Brownian motion model; K ≪ 1 means that closely related taxa resemble each other less

361   than expected under a Brownian motion model (such that variance is mostly found within

362   clades); finally, K ≫ 1 means that closely related units resemble each other more than

363   expected under a Brownian motion model (such that variance is mostly found among

364   clades).

365   <u>Phylomorphospace and reconstruction of ancestral morphotypes</u> To quantify and visualize

366   patterns of carotid canal course variation along the branches of the phylogeny, we produced

367   a phylomorphospace by projecting the phylogenetic tree onto the two first bgPCs

368   (Sidlauskas, 2008). In a phylomorphospace, the taxon centroids are connected to one

369   another in the morphospace following the phylogenetic relationships given by the chosen

370   phylogeny. In the case of fossil taxa, because there are competitive hypotheses regarding

371   their phylogenetic relationships, various time-calibrated cladograms were devised a priori—

372   resulting in a different phylomorphospace for each phylogenetic hypothesis. Scores of the

373   internal nodes—last common ancestors (LCAs)—were estimated based on a maximum

374   likelihood method for continuous characters using the 'fastAnc' function of 'phytools'. To

375   explore the extent to which extant and extinct taxa differ from the various LCAs, we rotated

376   and translated the bgPC scores estimated for the LCAs back into the Kendall's shape space

377   (i.e., configuration space) to obtain their landmarks coordinates and thus visualize the

378   estimated ancestral carotid canal course conformations.

379

380   **3. Results**

381   The 3D carotid canal surface of *Pliobates* (SOM File S2) is compared with those of

382   *Ekembo*, *Epipliopithecus*, and *Victoriapithecus*, as well as selected taxa from the extant

383 comparative sample in Figure 4. Individual data for the variables describing the orientation,

384 proportions, and course of the carotid canal in the extant comparative sample are reported

385 in SOM Table S2.

386

387 *3.1. Carotid canal orientation*

388 For 2DYZA, the angle values range from ca. 30° to 90° (Fig. 5a; Tables 3 and 4). On this

389 basis, and taking into account the mean extant clade differences (SOM Tables S3 and S4), we

390 defined three different states (potentially usable in future cladistic analyses): oblique (<55°);

391 subvertical (55–65°); and vertical (>65º). Hominoids have smaller angles than platyrrhines

392 and cercopithecids, i.e., a less vertically oriented canal, whereas cercopithecids have the

393 highest angles, corresponding to vertical canals (Fig. 5a; Table 3; SOM Tables S3 and S4).

394 *Pliobates* has the lowest value among Miocene catarrhines and does not significantly differ

395 from the hylobatid range of variation (Fig. 5a; Tables 4 and 5). *Epipliopithecus* and *Ekembo*

396 display very similar values to one another and most closely fit with the hominoid variation,

397 although they only significantly differ from cercopithecids (Fig.5a; Tables 4 and 5). In

398 contrast, *Victoriapithecus* has a higher angle, more similar to the monkey condition (i.e., a

399 more vertical canal; Fig.5a; Table 4), although it does not significantly differ from any extant

400 group (Table 5).

401 In the case of 2DXYA, the values range from ca. -4° to 45° (Fig. 5a; Tables 3 and 4; see

402 SOM S1 regarding the interpretation of negative angles). On this basis, and taking into

403 account the mean differences among extant clades (SOM Tables S3 and S4), we defined two

404 discrete states: anteriorly oriented (≤30°); and medially oriented (>30°). Despite some

405 overlap, platyrrhines display a significantly higher 2DXYA—i.e., a more medially (less

406 anteriorly) directed canal—than the three catarrhine families, which do not differ

17

407   significantly from one another (Fig. 5b; Table 3; SOM Tables S3 and S4). Among the fossil

408   specimens, *Ekembo* shows the highest 2DXYA whereas *Victoriapithecus* shows the lowest

409   (Fig.5b; Table 4). Based on the z-scores (Table 5), *Ekembo* displays a higher angle than extant

410   hominoids, *Victoriapithecus* and *Pliobates* show a lower angle than extant platyrrhines, and

411   *Epipliopithecus* displays a higher angle than hylobatids.

412

413   *3.2. Carotid canal proportions and body size scaling*

414   <u>Robusticity index</u> The two allometric regressions between L and $V^{1/3}$ are significant ($p <$

415   0.001; Table 6), but the PGLS regression indicates slight negative allometry, whereas the

416   major axis regression does not allow us to exclude isometry. This suggests that the canal

417   robusticity index $L/V^{1/3}$ is only slightly affected by intrinsic size-scaling effects, i.e., that

418   carotid canal length and volume covary in an almost linear fashion when geometric similarity

419   is considered. This is further confirmed by the lack of significant correlation between $L/V^{1/3}$

420   against CS (Table 6). When separate allometric regressions of L and $V^{1/3}$ against CS are

421   computed, it emerges that $V^{1/3}$ and CS display an isometric relationship, whereas L and CS

422   display a minimally positive allometric relationship (with a slope very close to 1). Overall, this

423   suggests that these three variables are suitable proxies for the size of the carotid canal and

424   that the robusticity index is only very slightly affected, if at all, by intrinsic size-scaling effects

425   related to the overall size of the canal.

426   Based on the robusticity index, and despite some overlap, platyrrhines display

427   significantly slenderer canals than catarrhine families, while hominids also display slenderer

428   canals than both cercopithecids and hylobatids, with the latter showing the stoutest canals

429   (Fig. 5c; Table 3; SOM Tables S3 and S4). *Ekembo* and *Epipliopithecus* exhibit similar indices,

430   while *Victoriapithecus* shows a somewhat higher value but similarly overlaps with all

18

431 catarrhine families (Fig. 5c; Table 4), and *Pliobates* shows an even higher value and falls

432 outside the hylobatid range (Fig. 5c; Table 4). However, none of the fossil specimens

433 significantly differs from any extant clade (Table 5).

434 <u>Body-size allometry</u> The fact that the robusticity index is not markedly affected by the size of

435 the canal itself notwithstanding, either carotid canal size and/or proportions could still be

436 affected by body size-scaling effects as measured by regressions against BM (Table 6). Both L

437 and CS display a negative allometric relationship relative to BM—slightly below the

438 theoretical isometric slope of 1/3 predicted by geometric similarity—whereas, in contrast,

439 $V^{1/3}$ fits well with the prediction of geometric isometry. This suggests that the volume of the

440 carotid canal is a better proxy for BM than either L or CS if size-scaling effects are not

441 corrected for, because the former variable is directly proportional to BM in a linear fashion,

442 whereas both L and CS display negative allometry relative to BM. The similar allometric

443 pattern of L and CS is not surprising, because the latter was computed from the carotid canal

444 configurations—which are sets of canal streampoints—and, hence, it only contains

445 information about carotid canal length (but not volume).

446 Differences in size scaling between L and V are reflected in the existence of a mild

447 negatively allometric relationship when L is considered the dependent variable, although

448 such a relationship is not significant when both variables are considered to display error (i.e.,

449 isometry cannot be excluded in the major axis regression; Table 6). Differences in scaling

450 between L and V relative BM, in any case, are reflected in the regression between the

451 robusticity index and BM (Table 6), which is of inverse proportionality (i.e., a negative slope):

452 since the numerator (L) of the index increases slightly slower than the denominator ($V^{1/3}$)

453 relative to BM, the index tends to decrease as the body size increases. However, it is

454 noteworthy that despite being significant, the correlation between the robusticity index and

455 body size only explains 14% of the variance (Table 6).

456

457 *3.3. Carotid canal course within the petrosal*

458 <u>Principal components analysis</u> The bgPCA discriminates between platyrrhines and

459 catarrhines but not among catarrhine families (Fig. 6). The cross-validated bgPCA (SOM Fig.

460 S3) is virtually identical to the standard bgPCA, and the permutational ANOVA results (SOM

461 Table S5) show that mean group differences are significant in all instances. The percentage

462 of variance explained by bgPCAs only increases slightly as compared with the raw data—

463 indicating that grouping structure is not spurious. The percentage of correctly classified

464 individuals by the bgPCA (Table 7) is moderately high (79%), even after cross-validation

465 (77%), although much higher in the case of platyrrhines (92%) and hominids (91%) than for

466 cercopithecoids (63%) and hylobatids (64%).

467 bgPC1 (Fig. 6a) explains most of the variance (94%), is not significantly correlated with CS

468 (p = 0.21; Table 6), and shows a strong phylogenetic signal at $p < 0.001$ (λ = 0.95; K = 3.28).

469 Although bgPC1 is not significantly correlated to ln CS, it displays significant allometry

470 relative to both $V^{1/3}$ and BM, but only explains 19% and 25% of the shape variance,

471 respectively (Table 6). This axis discriminates platyrrhines (negative scores) from catarrhines

472 (positive scores) at $p < 0.001$ (Fig. 5d; Table 3; SOM Tables S3 and S4) because of longer

473 canals that originate more inferolaterally in the petrosal of the former (Figs. 6b, 7; SOM Figs.

474 S4–S6). In contrast, catarrhines display shorter canals that originate more superiorly and are

475 overall located more medially in the petrosal (Figs. 6b and 7; SOM Figs. S4–S6). Extant

476 catarrhine families extensively overlap along bgPC1 and do not significantly differ in terms of

477 canal length and foramen/canal superoinferior and mediolateral position (Fig. 5d; Table 3;

478   SOM Tables S3 and S4). *Pliobates* and the remaining fossil taxa display similar (moderately

479   negative) bgPC1 scores that are intermediate between those of extant catarrhines and

480   extant platyrrhines (Figs. 5d and 6a; Table 4) and only slightly overlap with cercopithecids

481   and hominids or, in the case of *Epipliopithecus*, also marginally with platyrrhines. Their canal

482   configuration (SOM Figs. S4–S6) is thus somewhat shorter and more medially located than in

483   platyrrhines, although *Epipliopithecus* more closely resembles the platyrrhine condition than

484   *Pliobates*, *Victoriapithecus*, and *Ekembo* do.

485   bgPC2 (Fig. 6a) explains only 5% of variance, is significantly correlated with CS, $V^{1/3}$, and

486   BM (explaining respectively 58%, 46%, and 35% of the shape variance; Table 6), and shows

487   significant phylogenetic signal at $p < 0.001$ ($\lambda = 0.99$; K = 0.62). Variation along bgPC2 (Figs.

488   6b, 7) reflects the canal position on the petrosal (more anterior toward negative values, and

489   more posterior toward positive scores). Platyrrhines and catarrhines extensively overlap

490   along this axis, but hominids display significantly more positive values than other groups

491   despite considerable overlap (Fig. 5e; SOM Figs. S4–S6; SOM Tables S3 and S4). Along bgPC2,

492   *Epipliopithecus*, *Victoriapithecus* and *Ekembo* are found on slightly negative scores and

493   overlap with platyrrhines, cercopithecids and hylobatids, whereas *Pliobates* has a slightly

494   positive score that further overlaps with hominids (Figs. 5e and 6a; Table 4). The canal

495   configuration of *Pliobates* is thus somewhat more posteriorly located than in the other

496   extinct taxa (SOM Figs. S4–S6), particularly *Epipliopithecus*.

497   Z-scores (Table 5) indicate that, for bgPC1, *Epipliopithecus* significantly differs from all

498   extant groups, while other extinct taxa match the hominid distribution only. In contrast, for

499   bgPC2, *Epipliopithecus*, *Victoriapithecus* and *Ekembo* only significantly differ from hominids,

500   whereas *Pliobates* matches the variation of the four extant groups. When both bgPCs are

501   considered simultaneously, the analyzed extinct taxa differ from the four extant anthropoid

502   groups except for *Pliobates*, which matches the hominid variation. This is confirmed by

503   posterior probabilities of group membership (Table 8), according to which *Epipliopithecus*,

504   *Victoriapithecus*, and *Ekembo* are classified as cercopithecoids—although *Epipliopithecus*

505   falls outside their range of variation (p = 0.018)—whereas *Pliobates* is classified as a hominid

506   and only significantly differs from platyrrhines. According to these results, the canal course

507   of both *Ekembo* and *Victoriapithecus* fit better the cercopithecoid variation, whereas

508   *Pliobates* fits better with hominids, and *Epipliopithecus* does not fit well with any of the

509   extant groups analyzed. This notwithstanding, the results of the NJ cluster analysis (Fig. 8)

510   indicate that *Pliobates* and *Epipliopithecus* are most similar to one another. Indeed, the four

511   analyzed extinct taxa are grouped together in a cluster of their own, distinct from the

512   subcluster of great apes and that of platyrrhines.

513   The discrimination among the catarrhine families in the catarrhine-only bgPCA is slightly

514   better than in the analysis based on the whole sample but the three groups still overlap to

515   an important extent (SOM Fig. S7). The first axis explains most of the variance (85.33%) and

516   is the only one that discriminates between hominids and the remaining groups—as in the

517   whole sample analysis, in which only one axis (bgPC2) discriminates between them. The

518   results for the fossils in the catarrhine-only analysis are not more conclusive than for the

519   analysis including platyrrhines, with only minor differences. In particular, *Epipliopithecus* falls

520   closer to the hylobatid centroid and is classified as a hylobatid (p = 0.54), although it displays

521   no significant differences with either cercopithecids (p = 0.30) or hominids (p = 0.29);

522   *Victoriapithecus* still matches better the cercopithecid range of variation (p = 0.22), as it is

523   the case for *Ekembo* (p = 0.73), while *Pliobates* is classified first as a hominid (p = 0.39) but

524   also falls within the range of hylobatids (p = 0.14)—apparently owing to the more hominid-

525   like condition of *Symphalangus* as compared to other hylobatids.

526   <u>Phylomorphospace</u> The results of the phylomorphospace (Fig. 9; SOM Fig. S8) and the

527   reconstructed ancestral morphotypes (Fig. 10; SOM Fig. S9) are virtually identical

528   irrespective of the hypothesis considered. The crown platyrrhine LCA displays a very long

529   canal that originates inferiorly and is located very laterally in the petrosal (Fig. 10e; SOM Fig.

530   S9e), whereas the crown catarrhine LCA displays a condition almost indistinguishable from

531   the mean anthropoid configuration (Fig. 10f; SOM Fig. S9f). The inferred crown

532   cercopithecoid (Fig. 10g; SOM Fig. S9g) and crown hominoid (Fig. 10h; SOM Fig. S9h)

533   ancestral morphotypes are not very divergent from one another or from the catarrhine LCA,

534   but both are more derived than the latter by displaying a somewhat shorter and more

535   medially and posteriorly located canal. The crown hylobatid (Fig. 10i; SOM Fig. S9i) and

536   crown hominid (Fig. 10j; SOM Fig. S9j) LCAs more clearly diverge from the crown hominoid

537   LCA in different directions. Thus, the hylobatid LCA displays a higher bgPC1 score

538   overlapping with extant hylobatids and cercopithecoids, due to a shorter and more medially

539   located canal. In contrast, the hominid LCA displays a higher bgPC2 than the crown hominoid

540   LCA (like the extant hylobatid *Symphalangus*) due to a more posteriorly located canal.

541   The four analyzed extinct taxa are broadly similar to the crown catarrhine LCA's condition

542   (Fig. 9). Indeed, both *Victoriapithecus* (Fig. 10d) and *Ekembo* (Fig. 10c) most closely resemble

543   the crown catarrhine LCA rather than the crown ceropithecoid (Fig. 10g) or hominoid (Fig.

544   10h) LCAs. *Epipliopithecus* (Fig. 8b) displays a slightly more platyrrhine-like condition in

545   bgPC1 but is nevertheless very distinct from the crown platyrrhine LCA (Fig. 10e) and closer

546   to the inferred crown catarrhine ancestral condition. *Pliobates* (Fig. 10a) closely resembles

547   the crown catarrhine LCA in canal length and carotid foramen/canal superoinferior and

548   mediolateral position (as reflected in bgPC1), but unlike *Victoriapithecus* and *Ekembo* it

549   appears derived along bgPC2 toward the reconstructed ancestral hominid condition—albeit

550   being more similar along this axis to *Symphalangus* than to extant great apes—due to its

551   more posteriorly located canal.

552

553   **4. Discussion**

554   *4.1. Carotid canal orientation*

555   Two different characters were defined by Alba et al. (2015b: Tables S5 and S6) to code

556   the carotid canal morphology, one describing the canal 'orientation' (more or less

557   horizontal) and another (following Shoshani et al., 1996) describing the canal 'direction'

558   (more or less anterior). In Alba et al. (2015b), canal 'orientation' was defined as the

559   inclination between the canal and the basioccipital, whereas canal 'direction' was coded

560   based on the spatial relationship between the imaginary line emerging from the canal and

561   the foramen magnum. Canal 'direction' sensu Alba et al. (2015b) could be anterior or

562   posterior relative to the foramen magnum, i.e., more laterally or more anteriorly directed,

563   respectively. To evaluate this character, previous authors (Shoshani et al., 1996) placed a

564   straight wire inside the carotid canal and noted the point of intersection between the

565   imaginary line along the wire and the foramen magnum. In Alba et al. (2015b) on the other

566   hand, this character was evaluated conducting visual inspections on μCT scans, drawing the

567   course of the canal on basicranium inferior view and noting the point of intersection

568   between the imaginary line in continuation of the canal course and the foramen magnum.

569   2DYZA (canal superior orientation in the present study) is comparable with Alba et al.'s

570   (2015b) canal 'orientation' because this angle is measured along the parasagittal plan,

571   although based on values obtained we prefer to categorize them as

572   oblique/subvertical/vertical (as opposed to horizontal/oblique/subvertical as in Alba et al.,

573   2015b). In contrast, 2DXYA (canal medial orientation in the present study) is not directly

24

574 comparable with Alba et al.'s (2015b) canal 'direction', because while both studies rely

575 primarily on the line passing through the two canal endpoints (i.e., whole carotid canal), in

576 the present study the alignment process and the quantitative assessment of this character

577 (i.e., possibility of having more than two states vs. two qualitative states only in Alba et al.

578 [2015b]) make that this measure of canal orientation, for a same canal specimen, might

579 differ between the two studies.

580 *Pliobates* was coded by Alba et al. (2015b) as displaying a horizontal orientation

581 parallel to the basioccipital, like hylobatids, whereas the stem catarrhine *Saadanius*,

582 cercopithecoids (including *Victoriapithecus*) and hominids were coded with a subvertical

583 orientation, and *Epipliopithecus* and *Ekembo* with an intermediate (oblique) condition. Our

584 results for superior canal orientation (2DYZA) indicate that, in this regard, *Pliobates* does not

585 differ from hylobatids and display a lower value than *Ekembo* and *Epipliopithecus*. However,

586 our results further show that both hylobatids and hominids display a rather oblique

587 orientation (i.e., a horizontal orientation parallel to the basioccipital using the terminology of

588 Alba et al., 2015b), with *Ekembo* and *Epipliopithecus* resembling hominoids as a whole.

589 Nonetheless, all these taxa possess a less vertical orientation than platyrrhines (i.e., a

590 subvertical canal) and, especially, cercopithecoids (including *Victoriapithecus*), in which the

591 canal is vertical. To sum up, according to Alba et al. (2015b) hylobatids and *Pliobates* had a

592 horizontal canal, *Ekembo* and *Epipliopithecus* an oblique canal, and cercopithecoids

593 (including *Victoriapithecus*) and hominids a subvertical canal, whereas according to our

594 results all hominoids (including *Ekembo*), *Epipliopithecus*, and *Pliobates* have an oblique

595 canal, platyrrhines a subvertical canal, and cercopithecoids (including *Victoriapithecus*) an

596 even more vertical canal. Therefore, the superior orientation of the carotid canal is

597   consistent with the cercopithecoid status of *Victoriapithecus*, but it is not informative

598   regarding the stem catarrhine vs. stem hominoid status of *Pliobates.*

599   In turn, *Pliobates* was coded by Alba et al. (2015b) as resembling *Epipliopithecus* and

600   hylobatids in the 'direction' of the canal. The condition of all these taxa was coded as

601   anteriorly directed, the imaginary line emerging from the carotid canal crossing the foramen

602   magnum more posteriorly than in *Saadanius*, cercopithecids, and hominids, whose canal

603   would be more laterally directed, as in platyrrhines (see also Shoshani et al., 1996). In

604   contrast, our results indicate that hylobatids extensively overlap in canal medial orientation

605   with other extant catarrhines, which only significantly differ from platyrrhines. Furthermore,

606   *Pliobates* does not specifically resemble hylobatids or *Epipliopithecus*, but rather crown

607   catarrhines as a whole, including *Victoriapithecus*. On the other hand, *Epipliopithecus* and,

608   especially, *Ekembo,* exhibit a more platyrrhine-like condition, i.e., a medially directed canal.

609   To sum up, our results indicate that cercopithecoids (including *Victoriapithecus*), crown

610   hominoids, and *Pliobates* have an anteriorly oriented canal, whereas platyrrhines, *Ekembo*,

611   and *Epipliopithecus* have a medially oriented canal.

612

613   *4.2. Carotid canal proportions*

614   Volumetric proportions—which were not considered by Alba et al. (2015b)—as

615   measured by the robusticity index of the carotid canal, further confirm the differences in

616   carotid canal morphology between platyrrhines and catarrhines. Our allometric analyses

617   indicate that these differences cannot be explained by body size-scaling effects alone. In

618   particular, the volume of the carotid canal displays an isometric relationships with body size,

619   whereas length displays a slight negative allometric relationship with the latter. As a result,

620   larger-bodied taxa tend to display lower values of the robusticity index (i.e., slightly stouter

26

621 carotid canals). However, correlation with body mass only explains 14% of the variance in

622 carotid canal robusticity.

623   Based on our results, platyrrhines display on average slenderer canals (i.e., lesser

624 volume relative to length) than catarrhines. However, as for medial canal orientation,

625 catarrhine families largely overlap in canal proportions, although great apes display less

626 robust canals than cercopithecids and hylobatids, and are somewhat intermediate between

627 them and platyrrhines. The analyzed fossil catarrhines more closely resemble each other in

628 canal proportions than in canal orientation—being catarrhine-like but further overlapping

629 with the platyrrhine range of variation. *Pliobates* displays somewhat slenderer canals than

630 the other extinct taxa and, unlike them, it does not overlap with the hylobatids, even more

631 clearly than in the case of medial canal orientation thus further reinforcing the rejection of

632 possible closer similarities with hylobatids the latter family.

633   Our results for the extant taxa are in broad agreement with those previously obtained

634 by Boyer et al. (2016) on relative internal carotid artery area. Boyer et al. (2016) found

635 internal carotid area to scale isometrically with cranial area (measured as the square root of

636 the product between prosthion-inion length and bizygomatic breadth). Among catarrhines,

637 these authors found a pattern of decreasing robusticity in relative carotid artery area from

638 hylobatids to hominids, and to cercopithecids, which is the same as we found for the carotid

639 canal as a whole. The main difference between our results and those of Boyer et al. (2016) is

640 that, in the latter study, the carotid artery robusticity of platyrrhines was found to be

641 intermediate between hylobatids and hominids, whereas our results show that platyrrhines

642 have slenderer canals than catarrhines. This discrepancy is easily explained by the fact that

643 Boyer et al. (2016) considered internal carotid artery area relative to cranial area, whereas

644 we relied on the ratio between the length and the volume of the canal. Our results (see

645 below for further discussion) indicate that platyrrhines display relatively longer carotid

646 canals than catarrhines, thereby resulting in less robust volumetric proportions for the canal

647 as a whole. Given that Boyer et al. (2016) did not took canal length into account, this

648 explained the above-mentioned discrepancy for platyrrhines (but not the other groups) as

649 compared to our results.

650

651 *4.3. Carotid canal course*

652 Our bgPCA results indicate that the morphology of the canal embeds strong phylogenetic

653 signal, although most of the variance merely discriminates between platyrrhines and

654 catarrhines, due to differences in canal length and location reflected in bgPC1. In particular,

655 extant catarrhines display shorter canals that originate more superiorly than in platyrrhines.

656 It is noteworthy to stress beforehand that *Pliobates* and hylobatids do not show particular

657 similarities in bgPC1 scores.

658 Previous studies suggested that the carotid foramen is located ventrally (Ross, 1994; Ross

659 et al., 1998) and posteriorly (Ross, 1994; Ross et al., 1998; Kay et al., 2008) in both

660 platyrrhines and catarrhines, whereas Alba et al. (2015b) noted some differences in the

661 anteroposterior carotid foramen location between hylobatids and other catarrhines (with

662 the former displaying a more anteriorly located carotid foramen). Previous studies also

663 noted that platyrrhines display a more medially located foramen than catarrhines (Ross et

664 al., 1998; Kay et al., 2008). Our bgPC1 results indicate that extant platyrrhines and

665 catarrhines differ not only regarding the length of the canal, but also the location of the

666 (external) carotid foramen, such that in catarrhines the entire carotid canal (i.e., not only the

667 foramen but the whole structure) is more superiorly and medially located within the

668 petrosal. Our results therefore point to differences between platyrrhines and catarrhines in

669   terms of dorsoventral location of the carotid foramen, contrary to previous studies (Ross,

670   1994; Ross et al., 1998). This might be attributable to the different methodologies employed

671   (i.e., because of having performed an alignment on the specimens in the present study).

672   Similarly, because of the alignment, our conclusions for the location along the mediolateral

673   axis might be the opposite as those noted by previous authors (Ross et al., 1998; Kay et al.,

674   2008), who simply recorded foramen position relative to the bulla. Since catarrhines possess

675   a tubular ectotympanic, catarrhine landmark configurations are shifted more medially. This

676   is the consequence of alignment optimization of their tympanic landmarks with those of

677   platyrrhines, whose annular ectotympanic causes their tympanic landmarks to be more

678   medially positioned. Regardless, we observe an extensive overlap among extant catarrhine

679   families in the position of the carotid foramen, at least based on bgPC1.

680   Our results for bgPC2 lend some support that hylobatids display on average a more

681   anteriorly located foramen in the petrosal than hominids. However, rather than indicating a

682   particular condition for hylobatids, our bgPC2 results suggest that only hominids differ in this

683   regard from other catarrhines by displaying a more posteriorly located foramen. This

684   conclusion should be taken with caution, given that bgPC2 shows an extensive overlap

685   between hominids and the upper range of other crown catarrhines. Furthermore, bgPC2

686   reflects a smaller amount of variance, embeds lesser phylogenetic signal than bgPC1, and is

687   more strongly correlated with size—although the percentage of variance explained by

688   allometry varies depending on whether canal size or body size is considered, our results

689   clearly indicate that this axis is more strongly influenced by size-scaling than bgPC1.

690   Therefore, one should be cautious when interpreting similarities among taxa based on

691   bgPC2 scores.

692   Our 3DGM results for the analyzed fossil taxa do not support particular similarities

693 between *Pliobates* and hylobatids in terms of overall carotid canal course (contra Alba et al.,

694 2015b), and indicate instead that *Pliobates* is most similar in this regard to *Epipliopithecus*,

695 *Victoriapithecus* and *Ekembo*. All these fossil catarrhines appear overall closer to extant

696 catarrhines in terms of canal length and location in the petrosal, albeit being somewhat

697 intermediate between platyrrhines and catarrhines. *Epipliopithecus* appears slightly more

698 platyrrhine-like, whereas the other extinct genera only overlap with the lowest range of

699 cercopithecids and hominids (but not hylobatids). *Pliobates* only differs slightly from the

700 remaining fossil catarrhines by more closely resembling hominids and *Symphalangus* along

701 bgPC2 (reflecting a more posteriorly located foramen/canal). As noted above, bgPC2 is quite

702 strongly correlated with CS, suggesting that the differences between hominids and the rest

703 of the sample could merely result from the larger body size of the former. However, this

704 cannot explain the differences along this axis between *Pliobates* and *Epipliopithecus*, as the

705 former more closely resembles the large-bodied hominids and the largest-bodied hylobatid

706 (*Symphalangus*) despite a much lower estimated body size than *Epipliopithecus* (4–5 kg vs.

707 11–12 kg, respectively; Alba et al., 2015b).

708

709 *4.4. Evolutionary implications*

710   Alba et al. (2015b) concluded that *Pliobates* displays a mosaic of plesiomorphic (stem

711 catarrhine-like) cranial and postcranial features and more derived (crown hominoid) cranial

712 and postcranial synapomorphies, coupled with a dendropithecid-like dentition and some

713 cranial similarities with hylobatids. A stem hominoid status more derived than that of

714 *Ekembo* was supported for *Pliobates* by Alba et al. (2015b) based on the results of their

715   cladistic analysis. Such a phylogenetic placement would support the view that some

716   purported synapomorphies of crown catarrhines, best exemplified by the completely

717   ossified tubular ectotympanic, would have been independently acquired independently in

718   cercopithecoids and hominoids—a possibility taken into account by some previous authors

719   (Begun, 2002). A stem hominoid status for *Pliobates* would further support that the last

720   common ancestor of crown hominoids would have been more hylobatid-like than previously

721   assumed (Alba et al., 2015b). Interestingly, one of the resemblances between *Pliobates* and

722   hylobatids found by Alba et al. (2015b) was the carotid canal morphology, which is at odds

723   with the results of our more elaborate analyses of this anatomical structure, which denote a

724   generalized catarrhine morphology with some closer similarities with extant hominids and

725   uniquely *Symphalangus* among hylobatids.

726   Contrary to Alba et al. (2015b), subsequent cladistic analyses–based on different taxon-

727   character matrix–have recovered *Pliobates* as a stem catarrhine more closely related to

728   pliopithecoids (Nengo et al., 2017; Gilbert et al., 2020b). Based on these results, Gilbert et al.

729   (2020a: 399) concluded that "*Pliobates* is most likely a derived, late-occurring pliopithecoid

730   or other stem catarrhine taxon that has converged on some interesting but minor details of

731   extant hominoid elbows and wrists". In fact, the similarities in elbow and wrist morphology

732   between *Pliobates* and hominoids are not minor but quite extensive, more so than those

733   displayed by *Ekembo* and certainly than those convergently acquired by atelids (Alba et al.,

734   2015b). However, it is not unconceivable that these similarities—being functionally related

735   to enhanced forearm rotation and ulnar deviation capabilities—might have independently

736   evolved between *Pliobates* and crown hominoids. Under such scenario, in which postcranial

737   similarities between *Pliobates* and crown hominoids would be dismissed as convergences, it

738   should be taken into account that the dental morphology of *Pliobates* suggests much closer

739   affinities to dendropithecids (particularly *Micropithecus*) than to pliopithecoids (Alba et al.,

740   2015b). A dendropithecid status for *Pliobates* would not imply an independent acquisition of

741   a fully-ossified ectotympanic, but would not automatically resolve the phylogenetic

742   placement of the former, given the controversies surrounding the phylogenetic relationships

743   of dendropithecids—considered either stem catarrhines more derived than pliopithecoids

744   (Harrison, 2010, 2013, 2017; Nengo et al., 2017; Gilbert et al., 2020b) or stem hominoids

745   more basal than proconsulids (Rae, 1999; Zalmout et al., 2010; Begun, 2015; Alba et al.,

746   2015b; Rossie and Hill, 2018).

747   Unfortunately, the carotid canal morphology of dendropithecids is currently unknown,

748   thereby precluding a direct comparison with *Pliobates*. Furthermore, despite substantial

749   differences between platyrrhines and catarrhines in terms of carotid canal orientation and

750   proportions as well as carotid canal length and (foramen) location in the petrosal, our results

751   indicate a considerable overlap among extant catarrhines. As a result, carotid canal

752   morphology is of limited utility for investigating the phylogenetic position of fossil

753   catarrhines, although some insights can be drawn for the investigated taxa. Before

754   discussing the evolutionary implications of our results, however, it should be noted that the

755   small sample sizes available for extinct taxa make it necessary interpret the differences

756   among the analyzed fossil specimens by assuming that they are more or less representative

757   of their respective taxa. Although this caveat is not restricted to the carotid canal

758   morphology, it should not be forgotten that we cannot know a priori how similar in carotid

759   canal morphology a particular fossil specimen is to the (unknown) average condition of the

760   taxon to which it belongs. For example, given the considerable variation that can be

761   observed in some extant taxa for carotid canal course (e.g., *Aotus*, *Macaca*, *Mandrillus*), the

762   possibility remains that some of the differences inferred among extinct taxa, or between

763   them and extant catarrhine clades, might vanish (or become more accentuated) if additional

764   specimens became available. In the meantime, caution is required by bearing in mind that

765   the reliability of inferences for fossil taxa is limited by the number of specimens available to

766   them, which often preclude an adequate assessment of intraspecific variability.

767   Based on the currently available specimens, our results indicate that the stem hominoid

768   *Ekembo* and the stem cercopithecoid *Victoriapithecus* are virtually identical in carotid canal

769   volumetric proportions and course morphology, although *Ekembo* displays a more

770   platyrrhine-like medial orientation (like *Epipliopithecus*) and a more hominoid-like superior

771   orientation (like *Epipliopithecus* and *Pliobates* to some extent). The less medially/more

772   anteriorly oriented carotid canal in *Pliobates* than in *Ekembo* would be consistent with a

773   more derived stem hominoid status, but given the modern cercopithecoid-like carotid canal

774   orientation of *Victoriapithecus*, the condition of extant cercopithecoids and hominoids might

775   have evolved independently to some extent. In turn, based on the condition of

776   *Epipliopithecus*, the possession of an obliquely oriented canal in hominoids might represent

777   a catarrhine symplesiomorphy; in that case, the condition of extant cercopithecoids would

778   have independently evolved from that of extant platyrrhines. Alternatively, the oblique

779   orientation of the canal might be synapomorphic for hominoids, in which case the similar

780   condition of *Epipliopithecus* would be a convergence. Either way, this feature is not

781   informative regarding the phylogenetic position of *Pliobates*.

782   In terms of carotid canal course, as reflected by our 3DGM analysis, *Pliobates* does not

783   show particular affinities with hylobatids, and rather resembles the other analyzed extinct

784   taxa, which are overall more similar to catarrhines but somewhat intermediate between

785   platyrrhines and both cercopithecids and hominids. The phylomorphospace shows that both

786   *Victoriapithecus* and *Ekembo* apparently reflect well the inferred ancestral crown catarrhine

787   morphotype, despite their generally accepted crown catarrhine (respectively, stem

788   cercopithecoid and stem hominoid) status (e.g., Benefit and McCrossin, 1997; Benefit, 1999;

789   Alba et al., 2015b; Nengo et al., 2017; Gilbert et al., 2020b). In contrast, *Epipliopithecus*

790   appears somewhat more plesiomorphic, whereas *Pliobates* appears slightly derived (in the

791   anteroposterior position of the carotid foramen/canal) toward the great ape condition,

792   being closer to the inferred ancestral hominid morphotype as well as the hylobatid

793   *Symphalangus*.

794   In the case of *Epipliopithecus*, our results are in agreement with the widely held opinion

795   that pliopithecoids are a clade of stem catarrhines, predating the divergence of

796   cercopithecoids and hominoids (Harrison, 2013; Begun, 2002, 2017; Nengo et al., 2017;

797   Gilbert et al., 2020a, b; Sankhyan et al., 2017; Harrison et al., 2020; Urciuoli et al., 2021;

798   contra Alba et al., 2015b). For *Pliobates*, our results are more ambiguous and subject to

799   interpretation, although it is noteworthy that they do not support a closer relationship with

800   pliopithecoids—at least, based on the information provided by *Epipliopithecus*. They suggest

801   instead that, in carotid canal morphology, *Pliobates* is more derived than *Epipliopithecus*

802   toward the inferred ancestral crown catarrhine morphotype, like *Ekembo* and

803   *Victoriapithecus*. Furthermore, our results discount very close similarities in carotid canal

804   morphology between *Pliobates* and hylobatids as a whole, but indicate some resemblances

805   with the hylobatid *Symphalangus* and great apes. In the latter regard, *Pliobates* is

806   approximately equidistant from the crown catarrhine and crown hominoid reconstructed

807   morphotypes. It is uncertain whether this reflects a more derived status of *Pliobates* or an

808   independent development, although the latter is plausible in light of the *Symphalangus*

809   condition—if the hylobatid LCA reconstructed in the phylomorphospace is broadly correct,

810   *Symphalangus* must have independently acquired a more great ape-like condition; 811   alternatively, the condition shared by the hominid LCA and *Symphalangus* might be 812   plesiomorphic for crown hominoids and the reconstructed hylobatid LCA would reflect a 813   secondary reversal of the remaining hylobatids. Of course, the morphology of a single 814   anatomical region cannot provide much insight on the phylogenetic position of a given taxon 815   among catarrhines, particularly if—as it is the case of the carotid canal—it does not 816   adequately discriminate among catarrhine clades. However, our results for this structure do 817   not show any particular resemblances between pliopithecoids and *Pliobates* (beyond those 818   displayed by all the extinct taxa analyzed), and further fail to contradict the alternative 819   phylogenetic status of *Pliobates* as a stem hominoid. The phylogenetic status of *Pliobates* 820   thus seems far from being settled.

821

822   **5. Summary and conclusions**

823   Previous research on the primate carotid canal within a phylogenetic context has been 824   limited to the inclusion of qualitative features related to carotid foramen position in the 825   bulla and overall direction and orientation of the canal itself in character-taxon matrices 826   devised for cladistic analysis (Beard and MacPhee, 1994; Ross, 1994; Shoshani et al., 1996; 827   Ross et al., 1998; Kay et al., 2008; Alba et al., 2015b). From a quantitative viewpoint, only 828   Boyer et al. (2016) investigated the allometric relationship between carotid canal area and 829   BM (Boyer et al., 2016), whereas some authors relied on carotid canal area for inferring 830   encephalic blood flow rates and blood flow metabolism by further taking vertebral canal size 831   into account (Boyer and Harrington, 2018, 2019; Beaudet et al., 2020). Thus, our study is the 832   first to rigorously quantify the orientation, direction, overall course and volumetric

833   proportions of the carotid canal in 3D among a large sample of anthropoids. The allometric

834   regressions performed also represent an advancement in the understanding of body size-

835   scaling effects on carotid canal morphology. The methodological protocols devised here

836   enable repeatability among different researchers and thus will enable a refinement of our

837   conclusions by adding additional extant and fossil specimens in the future. The analyzed

838   variables are no panacea for clarifying the phylogeny of extinct catarrhines, because various

839   extant groups overlap to a large extent and also because intraspecific variation will be

840   difficult to evaluate due to small samples sizes. However, the analyzed variables offer the

841   prospect to provide taxonomically and phylogenetically relevant information for extinct taxa,

842   particularly if they are added to character-taxon matrices devised for cladistic analysis

843   including information from other anatomical areas. Other future directions of work on the

844   carotid canal should deepen our current understanding about the influence of function, as

845   well as allometric and phylogenetic constraints, on the evolution of this anatomical

846   structure. This would be required not only to better interpret carotid canal morphology from

847   an adaptive viewpoint, but also to derive from it paleobiological inferences for extinct taxa.

848   In this study, we rely on 3D morphometric techniques to quantify the orientation,

849   proportions, and course of the carotid canal in the small-bodied catarrhine *Pliobates*, and

850   compare it with extant anthropoids and other Miocene catarrhines (*Epipliopithecus*,

851   *Victoriapithecus,* and *Ekembo*). Our results reveal that *Pliobates* and the other analyzed

852   Miocene catarrhines are broadly similar to one another in carotid canal morphology and

853   more closely resemble extant catarrhines than platyrrhines. Unfortunately, carotid canal

854   morphology does not adequately discriminate among catarrhine clades, thereby hindering a

855   more detailed phylogenetic assessment of *Pliobates* on this basis. The difficulty of assessing

856   intraspecific variation in carotid canal morphology in the extinct taxa, coupled with the lack

857   of marked differences among extant catarrhine families, make it impossible to reach

858   definitive conclusions about the systematic position of *Pliobates* on this basis alone.

859   However, our results rule out the previously noted similarities in carotid canal morphology

860   between *Pliobates* and hylobatids and indicate instead that this extinct catarrhine is broadly

861   similar to catarrhines as a whole and, in particular, to other Miocene catarrhines (both stem

862   and crown).

863   It is however noteworthy that the carotid canal of *Pliobates* is not particularly similar to

864   that of pliopithecoids (as represented by *Epiplioithecus*, which appears somewhat more

865   platyrrhine-like), thereby not supporting (or contradicting) the hypothesis that *Pliobates* is a

866   pliopithecoid. Like the stem hominoid *Ekembo* and the stem cercopithecoid *Victoriapithecus*,

867   *Pliobates* appears somewhat more derived than *Epipliopithecus* toward the modern

868   catarrhine condition, and indeed, in some respects, *Pliobates* appears even more derived

869   toward the ancestral hominoid morphotype than the remaining Miocene catarrhines

870   analyzed, more closely resembling extant hominids and the hylobatid *Symphalangus*.

871   Therefore, our results do not enable us to discount the hypothesis that *Pliobates* is a stem

872   hominoid rather than a stem catarrhine. Given the dental similarities between *Pliobates* and

873   African dendropithecids, the former might be a late offshot of the latter clade that dispersed

874   into Eurasia independently from pliopithecoids. Unfortunately, this possibility could not be

875   directly assessed in this study because the carotid canal morphology of dendropithecids is

876   unknown. Additional analyses focused on other anatomical (both cranial and postcranial)

877   areas will be required to further clarify the phylogenetic relationships of *Pliobates*, as well as

878   to clarify whether its postcranial similarities with crown hominoids might have been

879   independently acquired.

912

References

914 Adams, D.C., Collyer, M.L., Kaliontzopoulou, A., 2019. Geomorph: Software for geometric

915 morphometric analyses. R Package Version 3.3.1. https://cran.r-

916 project.org/web/packages/geomorph/index.html.

917 Alba, D.M., Delson, E., Carnevale, G., Colombero, S., Delfino, M., Giuntelli, P., Pavia, M.,

918 Pavia, G., 2014a. First joint record of *Mesopithecus* and cf. *Macaca* in the Miocene of

919 Europe. J. Hum. Evol. 67, 1–18.

920 Alba, D.M., Colombero, S., Delfino, M., Martínez-Navarro, B., Pavia, M., Rook, L., 2014b. A

921 thorny question: The taxonomic identity of the Pirro Nord cervical vertebrae revisited. J.

922 Hum. Evol. 76, 92–106.

923 Alba, D.M., Montoya, P., Pina, M., Rook, L., Abella, J., Morales, J., Delson, E., 2015a. First

924 record of *Mesopithecus* (Cercopithecidae, Colobinae) from the Miocene of the Iberian

925 Peninsula. J. Hum. Evol. 88, 1–14.

926   Alba, D.M., Almécija, S., DeMiguel, D., Fortuny, J., Pérez de los Ríos, M., Pina, M., Robles,

927   J.M., Moyà-Solà, S., 2015b. Miocene small-bodied ape from Eurasia sheds light on

928   hominoid evolution. Science 350, aab2625.

929   Arnold, C., Matthews, L.J., Nunn, C.L., 2010. The 10kTrees website: A new online resource for

930   primate phylogeny. Evol. Anthropol. 19, 114–118.

931   Barry, J.C., Jacobs, L.L., Kelley, J., 1987. An early middle Miocene catarrhine from Pakistan

932   with comments on the dispersal of catarrhines into Eurasia. J. Hum. Evol. 15, 501–508.

933   Beard, K.C., MacPhee, R.D.E. 1994. Cranial anatomy of *Shoshonius* and the antiquity of

934   Anthropoidea. In: Fleagle, J.G., Kay, R.F. (Eds.), Anthropoid Origins. Plenum Press, New

935   York, pp. 55–97.

936   Beaudet, A., Clarke, R.J., Heaton, J.L., Pickering, T.R., Carlson, K.J., Crompton, R.H.,

937   Jashashvili, T., Bruxelles, L., Jakata, K., Bam, L., Van Hoorebeke, L., Kuman, K., Stratford,

938   D., 2020. The atlas of StW 573 and the late emergence of human-like head mobility and

939   brain metabolism. Sci. Rep. 10, 4285.

940   Begun, D.R., 2002. The Pliopithecoidea. In: Hartwig, W.C. (Ed.), The Primate Fossil Record.

941   Cambridge University Press, Cambridge, pp. 221–240.

942   Begun, D.R., 2015. Fossil record of Miocene hominoids. In: Henke, W., Tattersall, I. (Eds.),

943   Handbook of Paleoanthropology, 2nd ed. Springer, Heidelberg, pp. 1261–1332.

944   Begun, D.R., 2017. Evolution of the Pliopithecoidea. In: Fuentes, A. (Ed.), The International

945   Encyclopedia   of   Primatology.   John   Wiley   &   Sons,   Hoboken.

946   https://doi.org/10.1002/9781119179313.wbprim0165.

947   Benefit, B.R., 1999. *Victoriapithecus*: the key to Old World monkey and catarrhine origins.

948   Evol. Anthropol. 7, 155–174.

949   Benefit, B.R., McCrossin, M.L., 1997. Earliest known Old World monkey skull. Nature 388,

950   368–371.

951   Benefit, B.R., McCrossin, M.L., 2015. A window into ape evolution. Science 350, 515–516.

952   Bernor, R.L., Flynn, L.J., Harrison, T., Hussain, S.T., Kelley, J., 1988. *Dionysopithecus* from

953   southern Pakistan and the biochronology and biogeography of early Eurasian catarrhines.

954   J. Hum. Evol. 17, 339–358.

955   Blomberg, S.P., Garland, T., Ives, A.R., 2003. Testing for phylogenetic signal in comparative

956   data: behavioral traits are more labile. Evolution, 57, 717–745.

957   Bookstein, F.L., 1991. Morphometric Tools for Landmark Data: Geometry and Biology.

958   Cambridge University Press, Cambridge.

959   Boyer, D.M., Kirk, E.C., Silcox, M.T., Gunnell, G.F., Gilbert, C.C., Yapuncich, G.S., Allen, K.L.,

960   Welch, E., Bloch, J.I., Gonzales, L.A., Kay, R.F., Seiffert, E.R., 2016. Internal carotid arterial

961   canal size and scaling in Euarchonta: Re-assessing implications for arterial patency and

962   phylogenetic relationships in early fossil primates. J. Hum. Evol. 97, 123–144.

963   Boyer, D.M., Harrington, A.R., 2018. Scaling of bony canals for encephalic vessels in

964   euarchontans: Implications for the role of the vertebral artery and brain metabolism. J.

965   Hum. Evol. 114, 85–101.

966   Boyer, D.M., Harrington, A.R., 2019. New estimates of blood flow rates in the vertebral

967   artery of euarchontans and their implications for encephalic blood flow scaling: A

968   response to Seymour and Snelling (2018). J. Hum. Evol. 128, 93–98.

969   Bugge, J., 1974. The cephalic arterial system in insectivores, primates, rodents, and

970   lagomorphs, with special reference to the systematic classification. Acta Anat. 87, 1–160.

971   Bugge, J., 1980. Comparative anatomical study of the carotid circulation in New and Old

972   World Primates. In: Ciochon, R.L., Chiarelli, A.B. (Eds.), Evolutionary Biology of the New

973   World Monkeys and Continental Drift. Plenum Press, New York, pp. 293–316.

974   Cardini, A., O'Higgins, P., Rohlf, F.J., 2019. Seeing distinct groups where there are none:

975   spurious patterns from between-group PCA. Evol. Biol. 46, 303–316.

976   Cardini, A., Polly, P.D., 2020. Cross-validated between group PCA scatterplots: A solution to

977   spurious group separation? Evol. Biol. 47, 85–95.

978   Cartmill, M., MacPhee, R.D.E., Simons, E.L., 1981. Anatomy of the temporal bone in early

979   anthropoids, with remarks on the problem of anthropoid origins. Am. J. Phys. Anthropol.

980   56, 1–21.

981   Casanovas-Vilar, I., Alba, D.M., Garcés, M., Robles, J.M., Moyà-Solà, S., 2011. Updated

982   chronology for the Miocene hominoid radiation in Western Eurasia. Proc. Natl. Acad. Sci.

983   USA 108, 5554–5559.

984   Chatterjee, H.J., Ho, S.Y.W., Barnes, I., Groves, C. 2009. Estimating the phylogeny and

985   divergence times of primates using a supermatrix approach. BMC Evol. Biol. 13, 259.

986   Collyer, M.L., Adams, D.C., 2018. RRPP: An R package for fitting linear models to high-

987   dimensional data using residual randomization. Methods Ecol. Evol. 9, 1772–1779.

988   Delson, E., Terranova, C.J., Sargis, E.J., Jungers, W.L., Jablonski, N.G.C., Dechow, P., 2000.

989   Body mass in Cercopithecidae (Primates, Mammalia): estimation and scaling in extinct

990   and extant taxa. Anthropol. Pap. Am. Mus. Nat. Hist. 83, 1–159.

991   Diogo, R., Wood, B., 2011. Soft-tissue anatomy of the primates: Phylogenetic analyses based

992   on the muscles of the head, neck, pectoral region and upper limb, with notes on the

993   evolution of these muscles. J. Anat. 219, 272–359.

994 Finstermeier, K., Zinner, D., Brameier, M., Meyer, M., Kreuz, E., Hofreiter, M., Roos, C., 2013.

995 A mitogenomic phylogeny of living primates. PLoS One 8, e69504.

996 Gibbs, S., Collard, M., Wood, B., 2000. Soft-tissue characters in higher primate phylogenetics.

997 Proc. Natl. Acad. Sci. USA 97, 11130–11132.

998 Gibbs, S., Collard, M., Wood, B., 2002. Soft-tissue anatomy of the extant hominoids: A review

999 and phylogenetic analysis. J. Anat. 200, 3–49.

1000 Gilbert, C.C., Bibi, F., Hill, A., Beech, M.J., 2014. Early guenon from the late Miocene

1001 Baynunah Formation, Abu Dhabi, with implications for cercopithecoid biogeography and

1002 evolution. Proc. Natl. Acad. Sci. USA 111, 10119–10124.

1003 Gilbert, C.C., Pugh, K.D., Fleagle, J.G., 2020a. Dispersal of Miocene hominoids (and

1004 pliopithecoids) from Africa to Eurasia in light of changing tectonics and climate. In:

1005 Prasad, G.V., Patnaik, R. (Eds.), Biological Consequences of Plate Tectonics. New

1006 Perspectives on post-Gondwana Break-up—A Tribute to Ashok Sahni. Springer, Cham, pp.

1007 393-412.

1008 Gilbert, C.C., Ortiz, A., Pugh, K.D., Campisano, C.J., Patel, B.A., Premjit, N., Fleagle, J.G.,

1009 Patnaik, R., 2020b. New Middle Miocene ape (Primates: Hylobatidae) from Ramnagar,

1010 India fills major gaps in the hominoid fossil record. Proc. R. Soc. B. 287, 20201655.

1011 Gould, S.J., 1966. Allometry and size in ontogeny and phylogeny. Biol. Rev., 41, 587–640.

1012 Harrison, T., 2010. Dendropithecoidea, Proconsuloidea and Hominoidea (Catarrhini,

1013 Primates). In: Werdelin, L., Sanders, W.J. (Eds.), Cenozoic Mammals of Africa. University of

1014 California Press, Berkeley, pp. 429–469.

1015 Harrison, T., 2013. Catarrhine origins. In: Begun, D.R. (Ed.), A Companion to

1016 Paleoanthropology. Blackwell Publishing, Oxford, pp. 376–396.

1017   Harrison, T., 2016. The fossil record and evolutionary history of hylobatids. In: Reichard,

1018   U.H., Hirai, H., Barelli, C. (Eds.), Evolution of Gibbons and Siamang. Phylogeny,

1019   Morphology, and Cognition. Springer, New York, pp. 90–110.

1020   Harrison, T., 2017. Miocene primates. In: Fuentes, A. (Ed.), The International Encyclopedia of

1021   Primatology. John Wiley & Sons, Hoboken.

1022   https://doi.org/10.1002/9781119179313.wbprim0227.

1023   Harrison, T., Gu, Y., 1999. Taxonomy and phylogenetic relationships of early Miocene

1024   catarrhines from Sihong, China. J. Hum. Evol. 37, 225–277.

1025   Harrison, T., Zhang, Y., Wei, G., Sun, C., Wang, Y., Liu, J., Tong, H., Huang, B., Xu, F., 2020. A

1026   new genus of pliopithecoid from the late Early Miocene of China and its implications for

1027   understanding the paleozoogeography of the Pliopithecoidea. J. Hum. Evol. 145, 102838.

1028   Harzhauser, M., Kroh, A., Mandic, O., Piller, W. E., Göhlich, U., Reuter, M., Berning, B., 2007.

1029   Biogeographic responses to geodynamics: A key study all around the Oligo–Miocene

1030   Tethyan Seaway. Zool. Anz. 246, 241–256.

1031   Kay, R.F., Simons, E., Ross, J.L., 2008. The basicranial anatomy of African Eocene/Oligocene

1032   anthropoids. Are there any clues for platyrrhine origins? In: Fleagle, J.G., Gilbert, C.C.

1033   (Eds.), Elwyn Simons: A Search for Origins. Springer, New York, pp. 125–158.

1034   Legendre, P. 2018. lmodel2: Model II Regression. https://cran.r-

1035   project.org/web/packages/lmodel2/index.html.

1036   Lieberman, D.E., 1999. Homology and hominid phylogeny: Problems and potential solutions.

1037   Evol. Anthropol. 7, 142–151.

1038   Lieberman, D.E., McCarthy, R.C., 1999. The ontogeny of cranial base angulation in humans

1039   and chimpanzees and its implications for reconstructing pharyngeal dimensions. J. Hum.

1040   Evol. 36, 487–517.

1041 Lieberman, D.E., Ross, C.F., Ravosa, M.J., 2000. The primate cranial base: Ontogeny,

1042   function, and integration. Yearbk. Phys. Anthropol. 43, 117–169.

1043 MacPhee, R.D.E., Cartmill, M., 1986. Basicranial structures and primate systematics. In:

1044   Swisher, D.R., Erwin, J. (Eds.), Comparative Primate Biology: Systematics, Evolution, and

1045   Anatomy. Alan R. Liss, New York, pp. 219–275.

1046 McNulty, K.P., Begun, D.R., Kelley, J., Manthi, F.K., Mbua, E.N., 2015. A systematic revision of

1047   *Proconsul* with the description of a new genus of early Miocene hominoid. J. Hum. Evol.

1048   84, 42–61.

1049 Meyer, D., Rinaldi, Ir.D., Ramlee, H., Perwitasari-Farajallah, D., Hodges, J.K., Roos, C., 2011.

1050   Mitochondrial phylogeny of leaf monkeys (genus *Presbytis*, Eschscholtz, 1821) with

1051   implications for taxonomy and conservation. Mol. Phylogenet. Evol. 59, 311–319.

1052 Nengo, I., Tafforeau, P., Gilbert, C.C., Fleagle, J.G., Miller, E.R., Feibel, C., Fox, D.L., Feinberg,

1053   J., Pugh, K.D., Berruyer, C., Mana, S., Engle, Z., Spoor, F., 2017. New infant cranium from

1054   the African Miocene sheds light on ape evolution. Nature 548, 169–174.

1055 Pagel, M., 1999. Inferring the historical patterns of biological evolution. Nature 401, 877–

1056   884.

1057 Perelman, P., Johnson, W.E., Roos, C., Seuánez, H.N., Horvath, J.E., Moreira, M.A.M., Kessing,

1058   B., Pontius, J., Roelke, M., Rumpler, Y., Schneider, M.P.C., Silva, A., O'Brien, S.J., Pecon-

1059   Slattery, J., 2011. A molecular phylogeny of living primates. PLoS Genetics 7, e1001342.

1060 Pozzi, L., Hodgson, J.A., Burrell, A.S., Sterner, K.N., Raaum, R.L., Disotell, T.R., 2014. Primate

1061   phylogenetic relationships and divergence dates inferred from complete mitochondrial

1062   genomes. Mol. Phylogenet. Evol. 75, 165–183.

1063 R Core Team, 2020. R: A language and environment for statistical computing. R Foundation

1064   for Statistical Computing, Vienna.

1065   Rae, T.C., 1999. Mosaic evolution in the origin of the Hominoidea. Folia Primatol. 70, 125–

1066   135.

1067   Revell, L.J., 2012. *Phytools*: an R package for phylogenetic comparative biology (and other

1068   things). Methods Ecol. Evol. 3, 217–223.

1069   Roos, C., Kothe, M., Alba, D.M., Delson, E., Zinner, D., 2019. The radiation of macaques out

1070   of Africa: Evidence from mitogenome divergence times and the fossil record. J. Hum. Evol.

1071   133, 114–132.

1072   Rosenberger, A.L., Szalay, F., 1980. On the tarsiiform origins of the Anthropoidea. In:

1073   Ciochon, R.L., Chiarelli, A.B. (Eds.), Evolutionary Biology of the New World Monkeys and

1074   Contnental Drift. Plenum Press, New York, pp. 139–157.

1075   Ross, C., 1994. Evidence for anthropoid and tarsier relationships. In: Fleagle, J.G., Kay, R.F.

1076   (Eds.), Anthropoid Origins. Plenum Press, New York, pp. 469–547.

1077   Ross, C., Williams, B., Kay, R.F., 1998. Phylogenetic analysis of anthropoid relationships. J.

1078   Hum. Evol. 35, 221–307.

1079   Rossie, J.B., Hill, A., 2018. A new species of *Simiolus* from the middle Miocene of the Tugen

1080   Hills, Kenya. J. Hum. Evol. 125, 50–58.

1081   Sankhyan, A.R., Kelley, J., Harrison, T., 2017. A highly derived pliopithecoid from the Late

1082   Miocene of Haritalyangar, India. J. Hum. Evol 105, 1–12.

1083   Schlager, S., 2017. Morpho and Rvcg e shape analysis in R: R-packages for geometric

1084   morphometrics, shape analysis and surface manipulations. In: Zheng, G., Li, S., Székely, G.

1085   (Eds.), Statistical Shape and Deformation Analysis. Methods, Implementation and

1086   Applications.   Academic   Press,   London,   pp.   217–256.   https://cran.r-

1087   project.org/web/packages/Morpho/index.html.

1088   Schliep, K.P., 2011. phangorn: phylogenetic analysis in R. Bioinformatics 27, 592–593.

1089   Seiffert, E.R., 2006. Revised age estimates for the later Paleogene mammal faunas of Egypt

1090   and Oman. Proc. Natl. Acad. Sci. USA 103, 5000–5005.

1091   Seiffert, E.R., 2012. Early primate evolution in Afro-Arabia. Evol. Anthropol. 21, 239–253.

1092   Seiffert, E.R., Simons, E.L., Fleagle, J.G., Godinot, M., 2010. Paleogene anthropoids. In:

1093   Werdelin, L., Sanders, W.J. (Eds.), Cenozoic Mammals of Africa. University of California

1094   Press, Berkeley, pp. 369–391.

1095   Shoshani, J., Groves, C.P., Simons, E.L., Gunnell, G.F., 1996. Primate phylogeny:

1096   Morphological vs molecular results. Mol. Phylogenet. Evol. 5, 102–154.

1097   Sidlauskas, B., 2008. Continuous and arrested morphological diversification in sister clades of

1098   characiform fishes: aphylomorphospace approach. Evolution 62, 3135–3156.

1099   Smith, R.J., Jungers, W.L., 1997. Body mass in comparative primatology. J. Hum. Evol. 32,

1100   523–559.

1101   Springer, M.S., Meredith, R.W., Gatesy, J., Emerling, C.A., Park, J., Rabosky, D.L., Stadler, T.,

1102   Steiner, C., Ryder, O.A., Janečka, J.E., Fisher, C.A., Murphy, W.J., 2012. Macroevolutionary

1103   dynamics and historical biogeography of primate diversification inferred from a species

1104   supermatrix. PLoS One 7, e49521.

1105   Stevens, N.J., Seiffert, E.R., O'Connor, P.M., Roberts, E.M., Schmitz, M.D., Krause, C.,

1106   Gorscak, E., Ngasala, S., Hieronymus, T.L., Temu, J., 2013. Palaeontological evidence for

1107   an Oligocene divergence between Old World monkeys and apes. Nature 497, 611–614.

1108   Turner, T.R., Schmitt, C.A., Cramer, J.D., Lorenz, J., Grobler, J.P., Jolly, C.J., Freimer, N.B.,

1109   2018. Morphological variation in the genus *Chlorocebus*: Ecogeographic and

1110   anthropogenically mediated variation in body mass, postcranial morphology, and growth.

1111   Am. J. Phys. Anthropol. 166 (S3), 682–707.

1112 Urciuoli, A., Zanolli, C., Beaudet, A., Dumoncel, J., Santos, F., Moyà-Solà, S., Alba, D.M., 2020.

1113   The evolution of the vestibular apparatus in apes and humans. eLife 9, e51261.

1114 Urciuoli, A., Zanolli, C., Beaudet, A., Pina, M., Almécija, S., Moyà-Solà, S., Alba, D.M., 2021a. A

1115   comparative analysis of the vestibular apparatus in *Epipliopithecus vindobonensis*:

1116   Phylogenetic implications. J. Hum. Evol. 151, 102930.

1117 Urciuoli, A., Zanolli, C., Almécija, S., Beaudet, A., Dumoncel, J., Morimoto, N., Nakatsukasa,

1118   M., Moyà-Solà, S., Begun, D.R., Alba, D.M., 2021b. Reassessment of the phylogenetic

1119   relationships of the late Miocene apes *Hispanopithecus* and *Rudapithecus* based on

1120   vestibular morphology. Proc. Natl. Acad. Sci. USA 118, e2015215118.

1121 Walker, A., Teaford, M.F., Martin, L., Andrews, P., 1993. A new species of *Proconsul* from the

1122   early Miocene of Rusinga/Mfangano Islands, Kenya. J. Hum. Evol. 25, 43–53.

1123 Zalmout, I.S., Sanders, W.J., MacLatchy, L., Gunnell, G., Al-Mufarreh, Y.A., Ali, M.A., Nasser,

1124   A.-A.H., Al-Masary, A.M., Al-Sobhi, S.A., Nadhra, A.O., Matari, A.H., Wilson, J.A., Gingerich,

1125   P.D., 2010. New Oligocene primate from Saudi Arabia and the divergence of apes and Old

1126   World monkeys. Nature 466, 360–365.

1127 Zapfe, H., 1961. Die Primatenfunde aus der miozänen Spaltenfüllung von Neudorf an der

1128   March (Děvínská Nová Ves), Tschechoslowakei. Schweizer. Palaeontol. Abh. 78, 1–293.

1129

1130 **Figure captions**

1131

1132 **Figure 1.** Schematic illustration of the protocol used in this study for cutting the extremities

1133 of the carotid canal as exemplified in a *Macaca fascicularis* individual. a) To cut the posterior

1134 end, a best-fit plane defined for the landmarks placed at the carotid foramen is computed. b)

1135 To cut the anterior end, the 3D canal surface is first imported as a cloud of points in R. c) The

projection of IRG on the cloud of points (IRG′) is computed. d) 360 points are created around the axis IRG–IRG′. e, f) 360 possible cutting planes passing through IRG are created (each being based on IRG, IRG′ and one of the points rotating around the axis), here depicted in anterior (e) and superior (f) views. The cross-sectional area obtained by cutting the canal using each possible plane is calculated as follows: g–i) the points of the cloud belonging to the plane are recorded (g), the most external points (in red) are kept to create a convex hull that approximates the shape of the canal contour (h), and a set of triangles is drawn, each of them having the same point of the contour as the most acute vertex, and the two subsequent points on the contour as the other vertices (i); the total area is the obtained by summing those of each individual triangle. j, k) The plane with the smallest cross-sectional area (that is, orthogonal to the 3D canal surface and therefore to the canal streamline) (j) is used as a reference for cutting the canal at its anterior end (k). l) The centroids of the (posterior) carotid foramen landmark set and of the anterior cross-section (i.e., obtained by cutting with the orthogonal plane), representing the posterior and anterior endpoints of the carotid canal, respectively, are calculated. IRG = Intersection ridge–groove; IRG′ = orthogonal projection on the 3D carotid canal surface of IRG.

Figure 2. Petrosal landmarks used for aligning the specimens as exemplified in a *Macaca fascicularis* individual in different views: a) right lateral; b) inferior; c) sagittal cross section (right-mirrored for visualization purpose); d) superior transverse cross section. Landmarks: 1 = porion; 2 = inferior external auditory meatus; 3 = posterior external auditory meatus; 4 = posterior internal auditory meatus; 5 = anterior internal auditory meatus; 6 = medial anterior pyramidal ridge; 7 = intersection ridge-groove; 8 = greater superficial petrosal nerve hiatus; 9 = stylomastoid foramen.

1160

1161   **Figure 3.** Graphic representation of the 2D angles defining the carotid canal orientation

1162   relative to the cranium. a) Virtual external reconstructions of the cranium, in superior (left)

1163   and lateral (right) views. b) Virtual cross sections of the cranium to visualize the petrosal

1164   bone, in transverse (left) and sagittal (right) views. c) Representations of the carotid canal

1165   medial orientation (2DXYA; left) and superior orientation (2DYZA; right) within the cranium,

1166   rendered in semitransparency; red lines represent the 2D canal vector and its direction,

1167   orange squares represent the plane along which the angle can vary, and dotted black lines

1168   represent the standard reference vector. For 2DXYA, the plane of angle variation is a

1169   transverse plane, whereas for 2DYZA the plane of angle variation is a (para)sagittal plane.

1170   For both angles, the standard reference vector is a 2D vector parallel to the anteroposterior

1171   cranial axis (from posterior to anterior). Both angles are calculated between the 2D canal

1172   vector and the 2D standard reference vector. Because the anthropoid mean configuration is

1173   extremely similar to the canal course configuration of *Presbytis* (i.e., before alignment), the

1174   cranium of this taxon is used as a reference for orienting the canal following the cranial axes

1175   of reference.

1176

1177   **Figure 4.** Virtual reconstructions of carotid canal comparing *Pliobates* with extant

1178   anthropoids and some Miocene catarrhines: a) *Pliobates* (IPS58443.1); b) *Epripliopithecus*

1179   (NHMW 1970/1397/0003); c) *Ekembo* (KNM-RU 2036al); d) *Victoriapithecus* (KNM-MB

1180   29100); e) *Alouatta*; f) *Aotus*; g) *Cebus*; h) *Mico*; i) *Plecturocebus*; j) *Cercopithecus*; k)

1181   *Colobus*; l) *Mandrillus*; m) *Presbytis*; n) *Hylobates*; o) *Hoolock*; p) *Nomascus*; q)

1182   *Symphalangus*; r) *Gorilla*; s) *Pan*; t) *Pongo*. The canals are shown in medial view with their

1183   posterior ends horizontally aligned. Scale bars = 5 mm.

1184

1185   **Figure 5.** Box-and-whisker plots of the variables describing the orientation, proportions and

1186   course of the carotid canal in the fossil specimens and main extant clades analyzed in this

1187   study: a) 2D YZ angle; b) 2D XY angle; c) index $L/V^{(1/3)}$; d) bgPC1; e) bgPC2. Horizontal lines

1188   denote medians, boxes depict the interquartile range, whiskers the minimum-maximum

1189   values excluding outliers, dots denote outliers (beyond 1.5 times above or below the

1190   interquartile range). Abbreviations: L = length (in mm); V = volume (in mm^3); bgPC =

1191   between-group principal component; 2DYZA = 2D angle in the YZ plane (canal superior

1192   orientation; in degrees); 2DXYA = 2D angle in the XY plane (canal medial orientation; in

1193   degrees).

1194

1195   **Figure 6**. Results of the between-group principal component analysis (bgPCA) based on

1196   carotid canal course variation among main extant anthropoid clades. a) Bivariate plot of

1197   bgPC2 vs. bgPC1 (the variance explained by each bgPC is denoted in parentheses). b)

1198   Minimum (blue) and maximum (red) landmark conformations compared with the

1199   anthropoid mean configuration (black) for bgPC1 and bgPC2, in superior (top), lateral

1200   (middle), and anterior (bottom) views (anatomical axes of reference are specified next to

1201   each view; see Fig. 7 for a representation of the carotid canal within the cranium). Convex

1202   hulls correspond to: platyrrhines (blue), cercopithecids (red), hylobatids (green), and

1203   hominids (gray). Abbreviation: bgPC = between-group principal component.

1204

1205   **Figure 7.** Representations of the carotid canal relative to the cranium in superior (left),

1206   lateral (middle), and anterior (right) views. a) Virtual external reconstruction of the cranium.

1207   b) Virtual cross sections of the cranium to visualize the petrosal bone (from left to right,

1208 transverse, sagittal, and coronal sections are depicted). c) Virtual reconstructions of the

1209 carotid canal within the cranium rendered in semitransparency. d, e) Minimum (blue) and

1210 maximum (red) landmark conformations compared with the anthropoid mean configuration

1211 (black) for bgPC1 (d) and bgPC2 (e) within the cranium rendered in semitransparency.

1212 Because the anthropoid mean configuration is extremely similar to the canal course

1213 configuration of *Presbytis* (i.e., before alignment), the cranium of this taxon is used as a

1214 reference for orienting the canal following the cranial axes of reference.

1215

1216 **Figure 8.** Neighbor-joining cluster (unrooted) based on the Euclidean distances calculated

1217 from raw coordinates of the canal course configurations in *Pliobates*, extant anthropoids and

1218 other Miocene catarrhines. Cophenetic = 0.94.

1219

1220 **Figure 9.** Phylomorphospace of carotid canal course variation in extant anthropoids and

1221 extinct Miocene catarrhines including *Pliobates. Epipliopithecus* and *Pliobates* are considered

1222 sister taxa within a stem catarrhine pliopithecoid clade and *Ekembo* is considered a stem

1223 hominoid while *Victoriapithecus* is considered a stem cercopithecoid (see SOM Fig. S2b for a

1224 representation of this phylogenetic hypothesis). Ancestral nodes: 1 = crown platyrrhines; 2 =

1225 crown catarrhines; 3 = crown cercopithecoids; 4 = crown hominoids; 5 = crown hominids; 6 =

1226 crown hylobatids. See SOM Figure S8 for a phylomorphospace derived from the alternative

1227 phylogenetic hypothesis (SOM Fig. S2b).

1228

1229 **Figure 10.** Configurations of the carotid canal course in *Pliobates* compared with other

1230 Miocene catarrhines and the reconstructed carotid canal course for the last common

1231 ancestors (LCAs) of various anthropoid clades: a) *Pliobates* (IPS58443.1); b) *Epipliopithecus*

1232   (NHMW 1970/1397/0003); c) *Ekembo* (KNM-RU 2036al); d) *Victoriapithecus* (KNM-MB

1233   29100); e) crown platyrrhines; f) crown catarrhines; g) crown cercopithecoids; h) crown

1234   hominoids; i) crown hylobatids; j) crown hominids. The canal courses of the LCAs have been

1235   inferred based on the phylomorphospace displayed in Figure 9 (see SOM Fig. S9 for the

1236   inferred LCA configurations derived from the alternative phylogenetic hypothesis). For each

1237   specimen/LCA, the configurations are displayed in superior (left), lateral (middle), and

1238   anterior (right) views. The mean configuration computed for the whole anthropoid sample is

1239   represented by black dots, while configurations for Miocene catarrhines and LCAs are

1240   represented in beige. The anthropoid mean configuration was used as a reference for

1241   visualizing all the configurations at the same relative scale.

1242

a

b

IRG

c

IRG'

d

e

f

g

h

i

j

k

l

10 mm
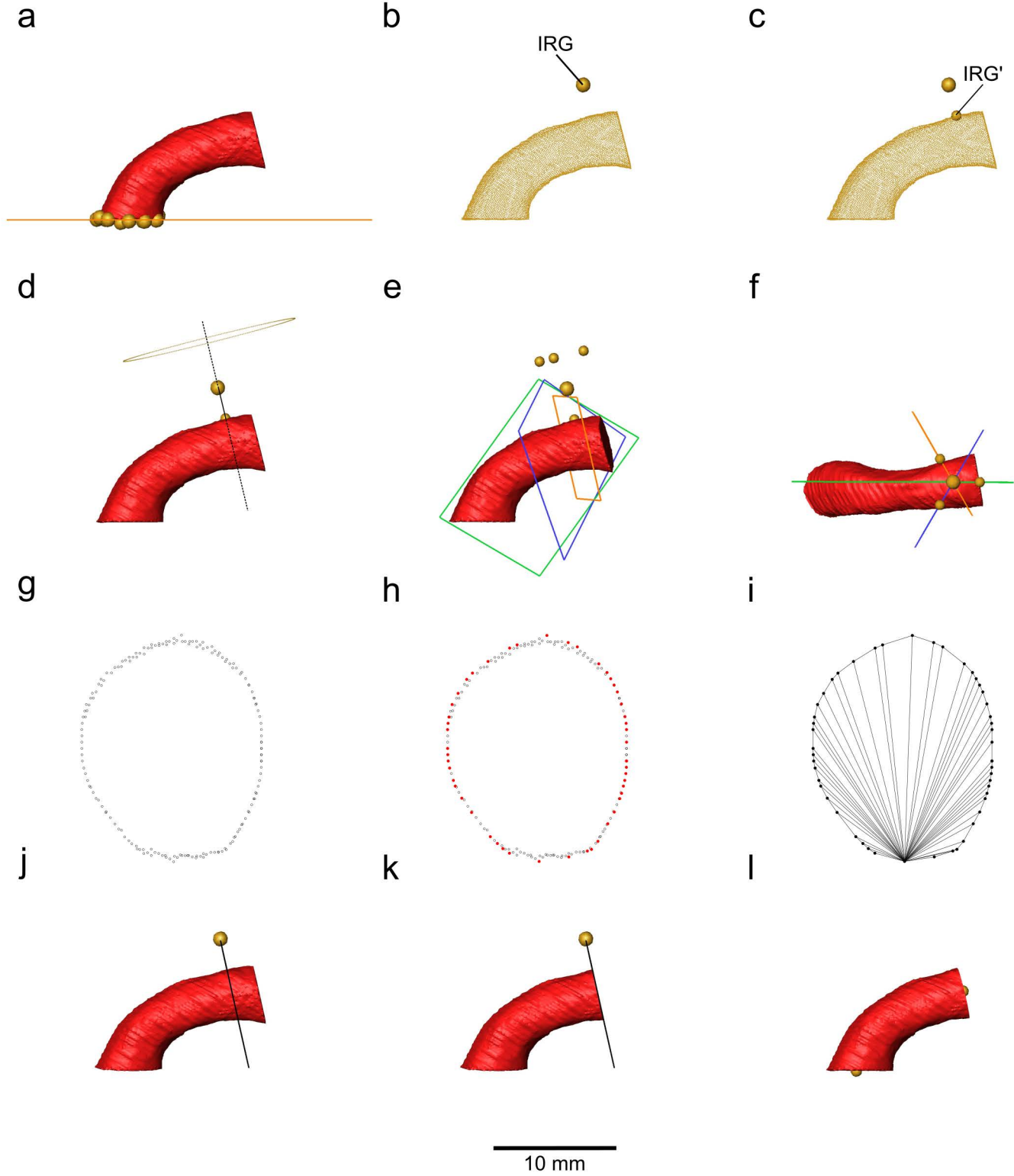
a
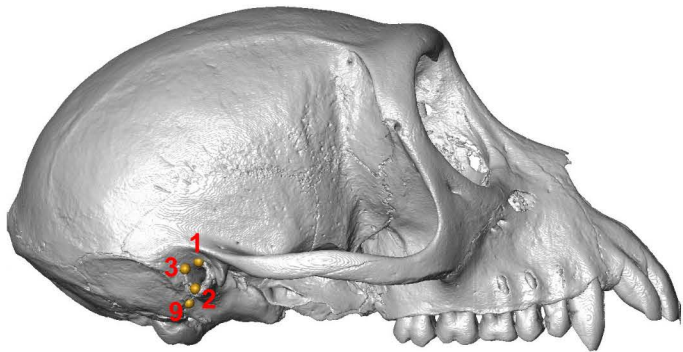
b
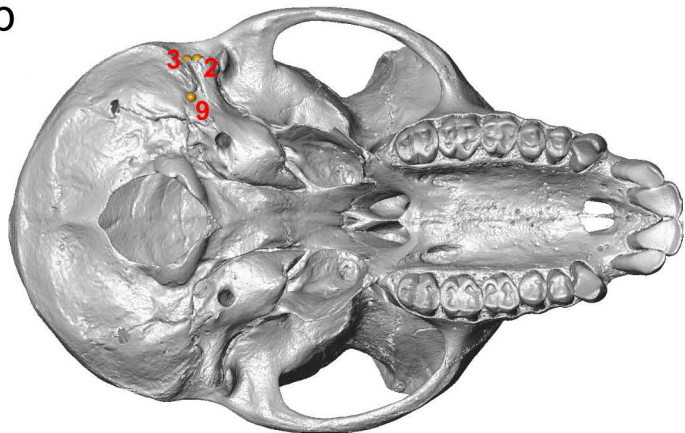
c
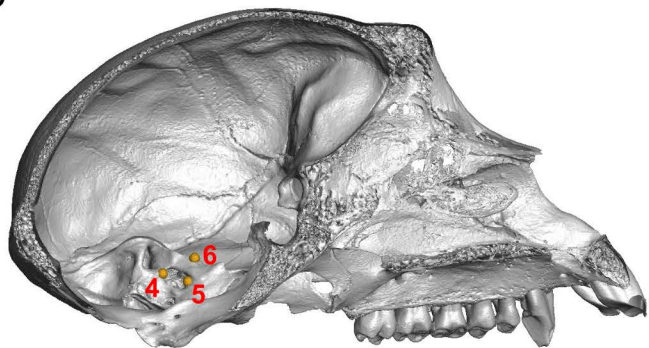
d
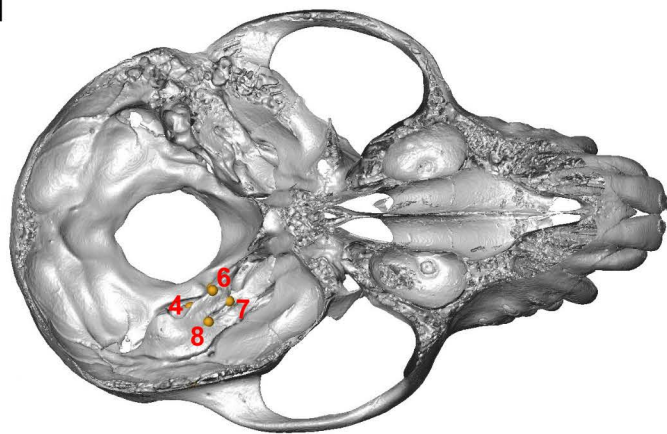
50 mm

a
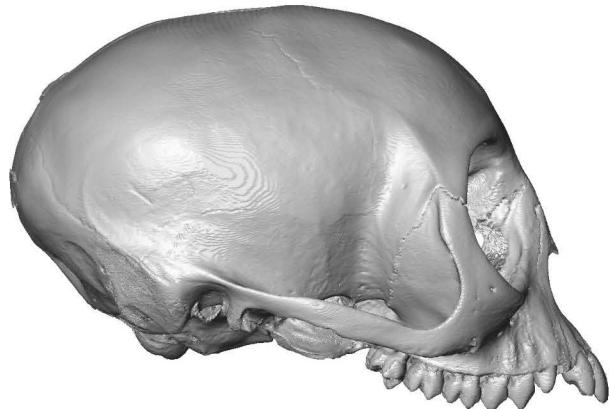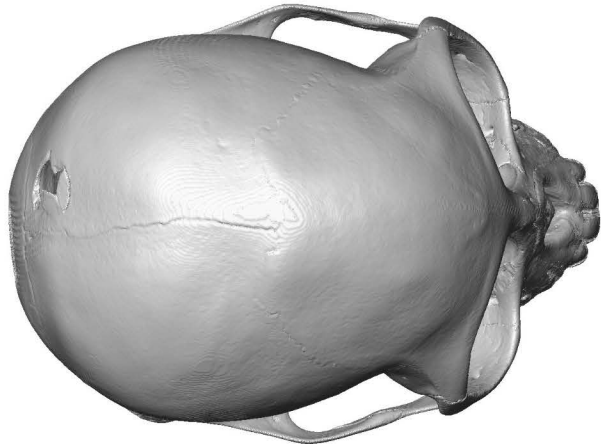
b
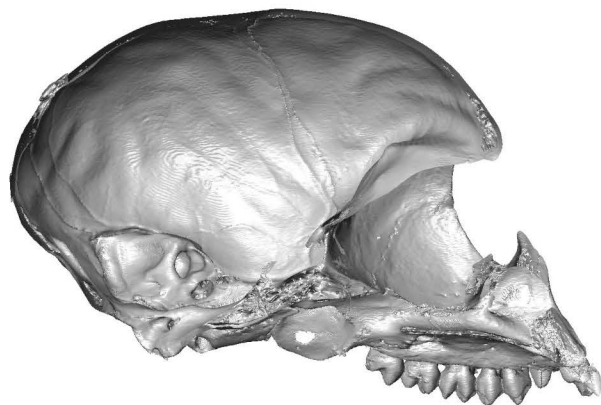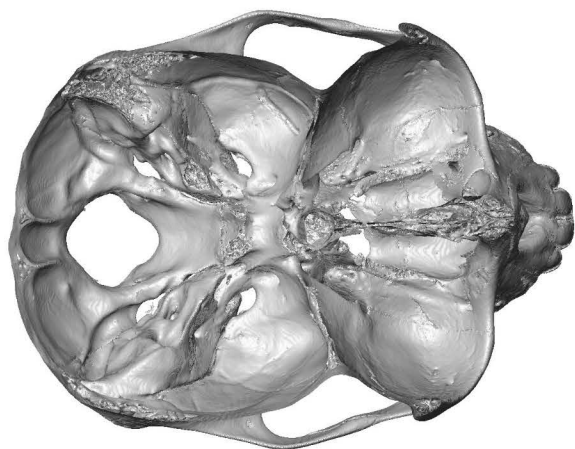
c
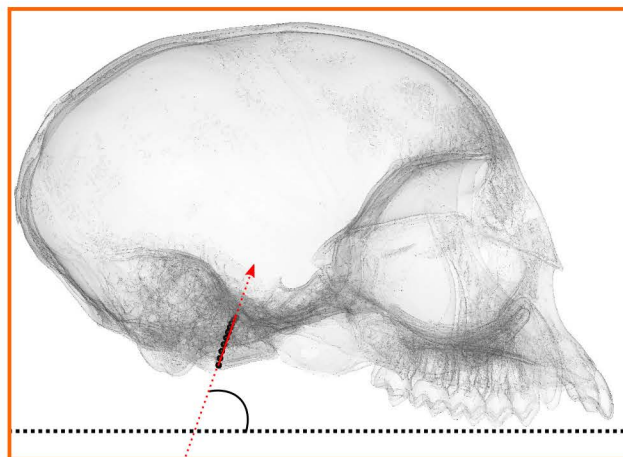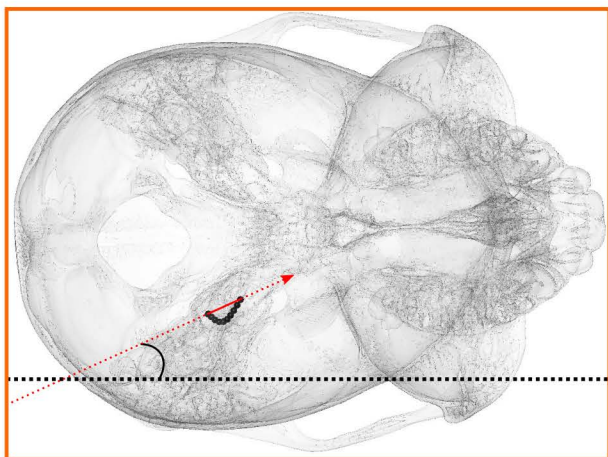
50 mm
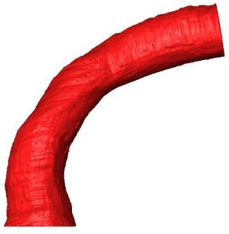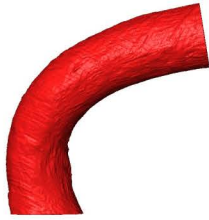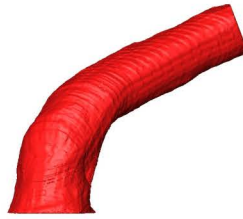
a) *Pliobates*   b) *Epipliopithecus*   c) *Ekembo*   d) *Victoriapithecus*

e) *Alouatta*   f) *Aotus*   g) *Cebus*   h) *Mico*
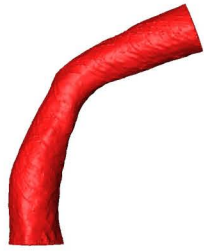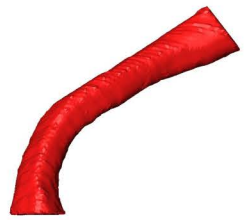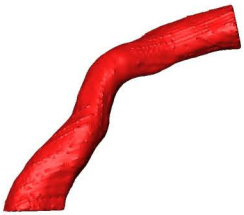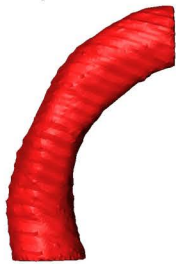
i) *Plecturocebus*   j) *Cercopithecus*   k) *Colobus*   l) *Mandrillus*
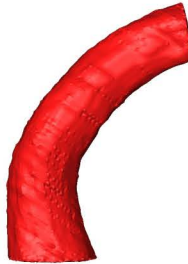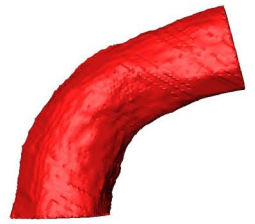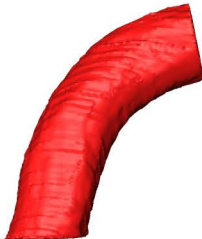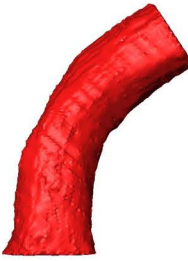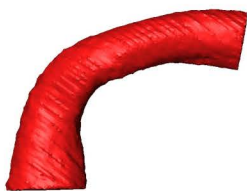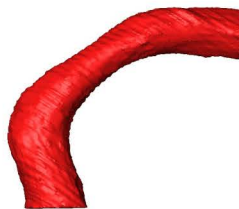
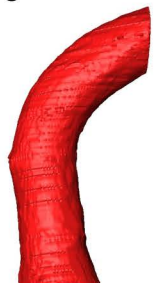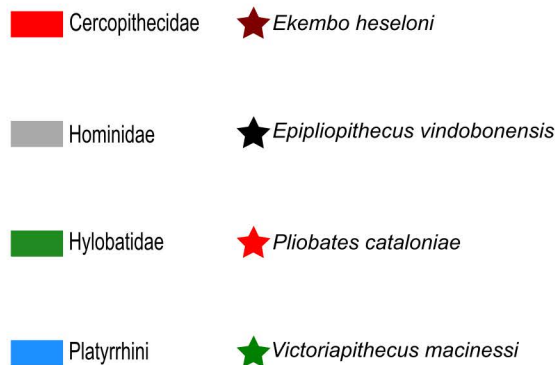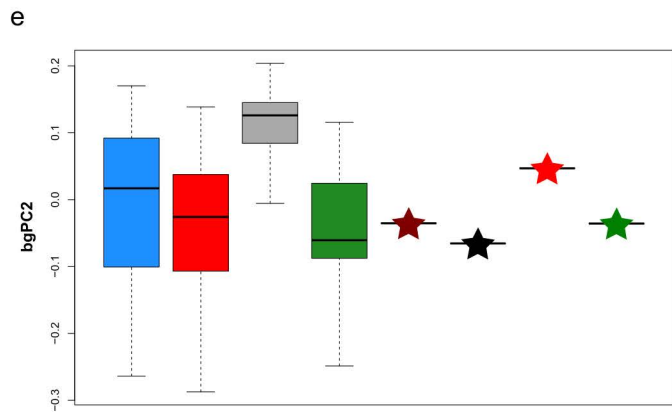m) *Presbytis*   n) *Hylobates*   o) *Hoolock*   p) *Nomascus*

q) *Symphalangus*   r) *Gorilla*   s) *Pan*   t) *Pongo*

a

2DYZA (degrees)

b

2DXYA (degrees)

c

Index L/V$^{(1/3)}$

d

bgPC1

e

bgPC2

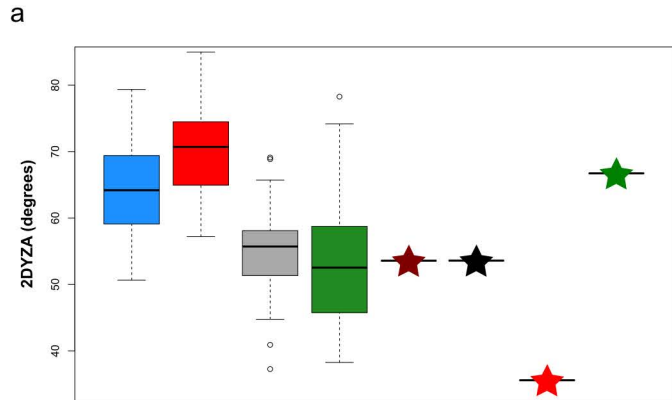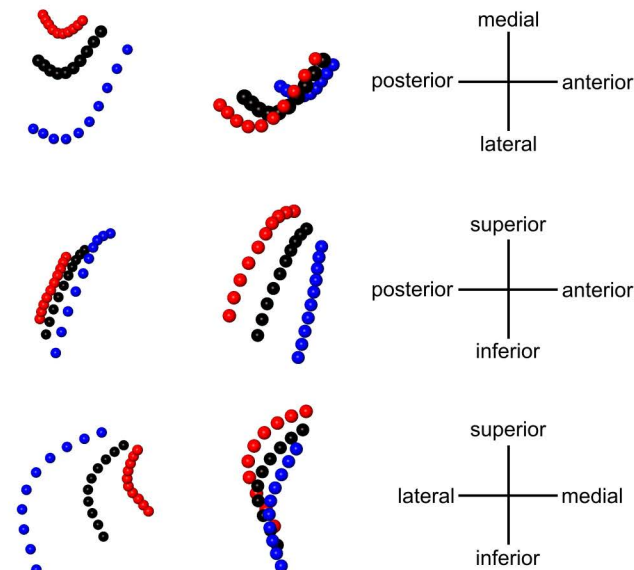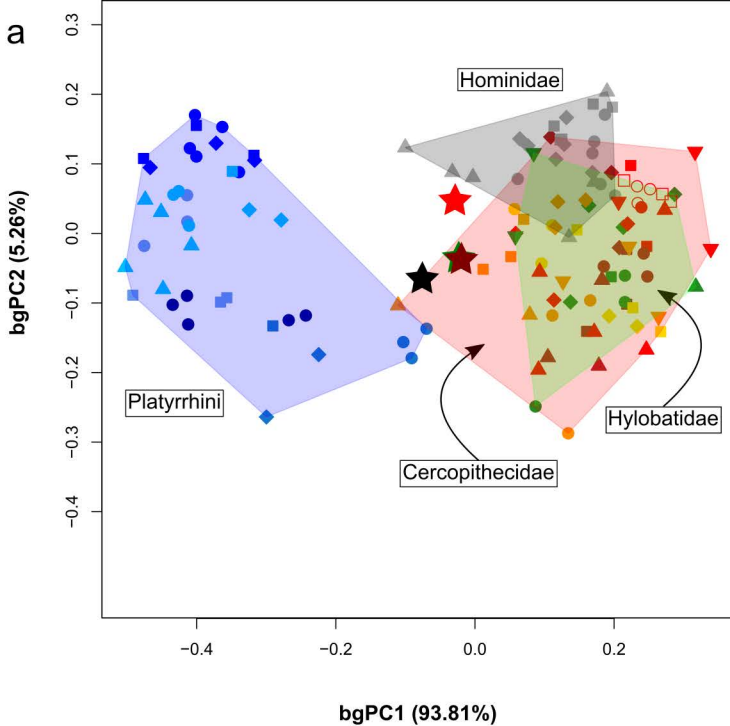|	
■ Cercopithecidae	★ *Ekembo heseloni*
■ Hominidae	★ *Epipliopithecus vindobonensis*
■ Hylobatidae	★ *Pliobates cataloniae*
■ Platyrrhini	★ *Victoriapithecus macinessi*

a

Legend:

- *Alouatta palliata*
- *Ateles geoffroyi*
- *Lagothrix lagotricha*

- *Aotus griseimembra*

- *Mico argentatus*
- *Saguinus fuscicollis*
- *Saguinus midas*

- *Cebus imitator*
- *Saimiri sciureus*

- *Chiropotes chiropotes*
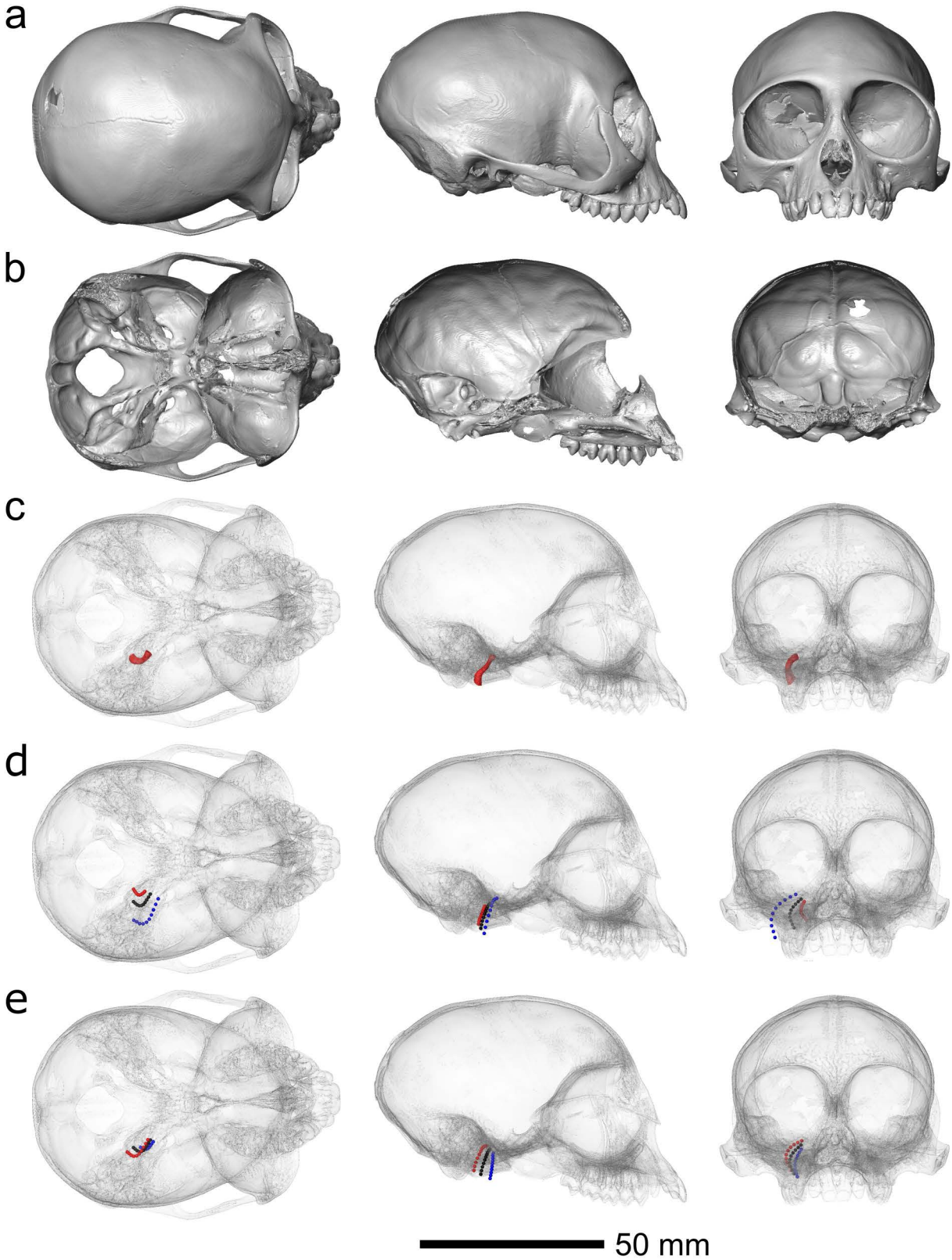- *Pithecia monachus*
- *Pithecia pithecia*
- *Plecturocebus cupreus*

- *Cercocebus galeritus*
- *Cercocebus torquatus*
- *Lophocebus albigena*
- *Macaca fascicularis*
- *Mandrillus sphinx*
- *Papio anubis*
- *Theropithecus gelada*

- *Cercopithecus mitis*
- *Chlorocebus pygerythrus*
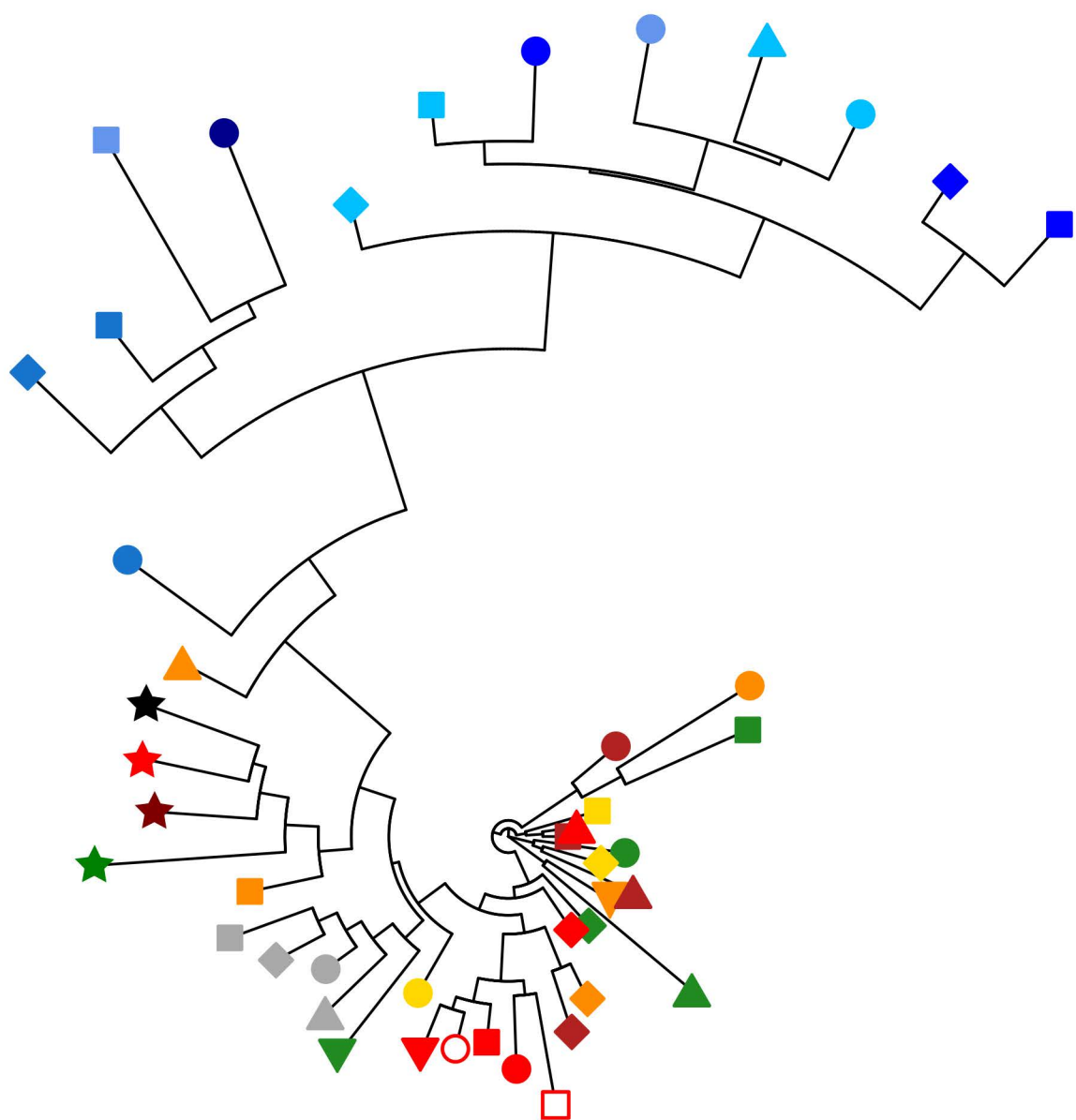- *Erythrocebus patas*
- *Miopithecus talapoin*

- *Colobus guereza*
- *Piliocolobus badius*
- *Procolobus verus*

- *Nasalis larvatus*
- *Presbytis rubicunda*
- *Semnopithecus entellus*
- *Simias concolor*
- *Trachypithecus cristatus*

- *Gorilla gorilla*
- *Pan paniscus*
- *Pan troglodytes*
- *Pongo* sp.

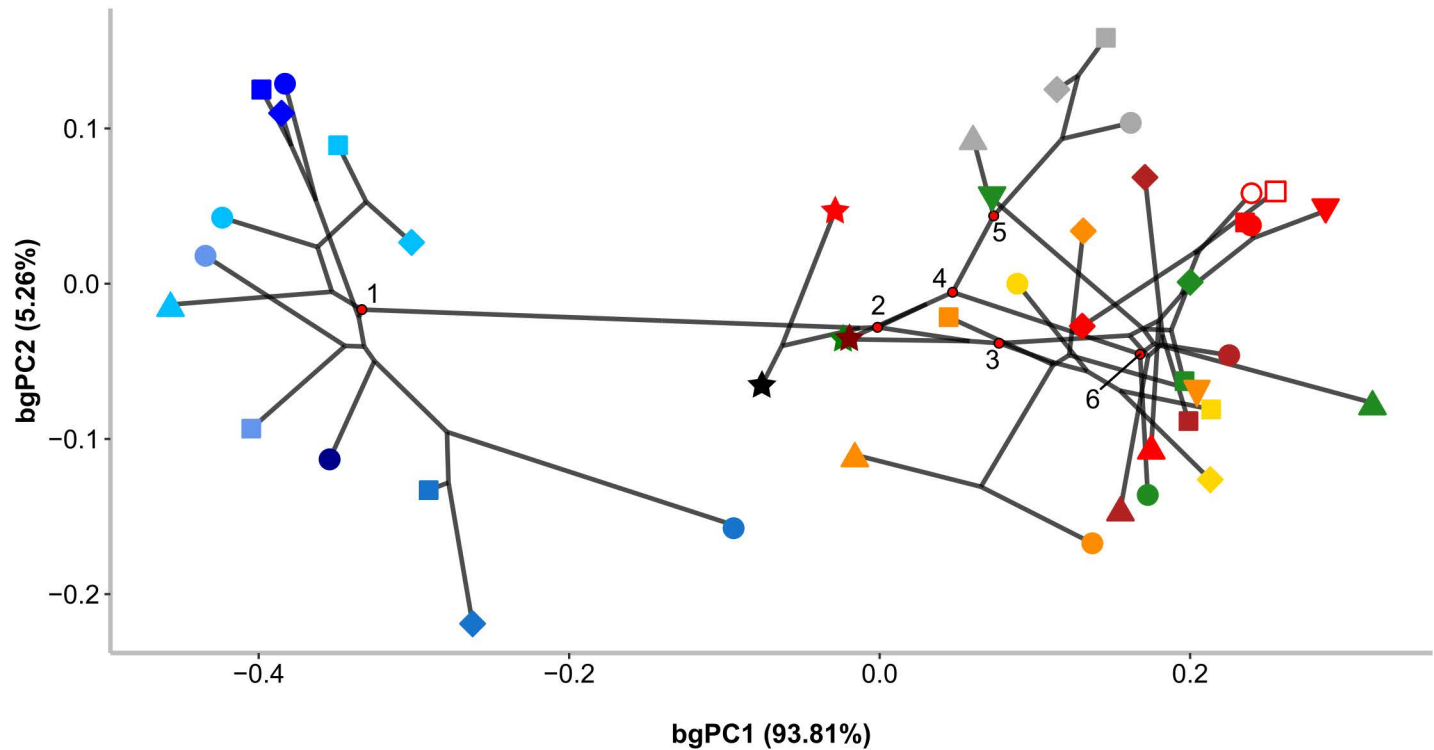- *Hoolock hoolock*
- *Hylobates agilis*
- *Hylobates lar*
- *Nomascus leucogenys*
- *Symphalangus syndactylus*

- *Ekembo heseloni*
- *Epipliopithecus vindobonensis*
- *Pliobates cataloniae*
- *Victoriapithecus macinessi*

a

b

c

d

e

50 mm

Alouatta palliata
Ateles geoffroyi
Lagothrix lagotricha

Aotus griseimembra

Mico argentatus
Saguinus fuscicollis
Saguinus midas

Cebus imitator
Saimiri sciureus

Chiropotes chiropotes
Pithecia monachus
Pithecia pithecia
Plecturocebus cupreus

Cercocebus galeritus
Cercocebus torquatus
Lophocebus albigena
Macaca fascicularis
Mandrillus sphinx
Papio anubis
Theropithecus gelada

Cercopithecus mitis
Chlorocebus pygerythrus
Erythrocebus patas
Miopithecus talapoin

Colobus guereza
Piliocolobus badius
Procolobus verus

Nasalis larvatus
Presbytis rubicunda
Semnopithecus entellus
Simias concolor
Trachypithecus cristatus

Gorilla gorilla
Pan paniscus
Pan troglodytes
Pongo sp.

Hoolock hoolock
Hylobates agilis
Hylobates lar
Nomascus leucogenys
Symphalangus syndactylus

Ekembo heseloni
Epipliopithecus vindobonensis
Pliobates cataloniae
Victoriapithecus macinessi

● *Alouatta palliata*	● *Cercocebus galeritus*	● *Colobus guereza*	● *Gorilla gorilla*	★ *Ekembo heseloni*
■ *Ateles geoffroyi*	■ *Cercocebus torquatus*	■ *Piliocolobus badius*	■ *Pan paniscus*	★ *Epipliopithecus vindobonensis*
◆ *Lagothrix lagotricha*	◆ *Lophocebus albigena*	◆ *Procolobus verus*	◆ *Pan troglodytes*	★ *Pliobates cataloniae*
	▲ *Macaca fascicularis*		▲ *Pongo* sp.	★ *Victoriapithecus macinessi*
● *Aotus griseimembra*	▼ *Mandrillus sphinx*	● *Nasalis larvatus*		
	○ *Papio anubis*	■ *Presbytis rubicunda*	● *Hoolock hoolock*	
● *Mico argentatus*	□ *Theropithecus gelada*	◆ *Semnopithecus entellus*	■ *Hylobates agilis*	
■ *Saguinus fuscicollis*		▲ *Simias concolor*	◆ *Hylobates lar*	
◆ *Saguinus midas*	● *Cercopithecus mitis*	▼ *Trachypithecus cristatus*	▲ *Nomascus leucogenys*	
	■ *Chlorocebus pygerythrus*		▼ *Symphalangus syndactylus*	
● *Cebus imitator*	◆ *Erythrocebus patas*			
■ *Saimiri sciureus*	▲ *Miopithecus talapoin*			
● *Chiropotes chiropotes*				
■ *Pithecia monachus*				
◆ *Pithecia pithecia*				
▲ *Plecturocebus cupreus*				

a) *Pliobates*
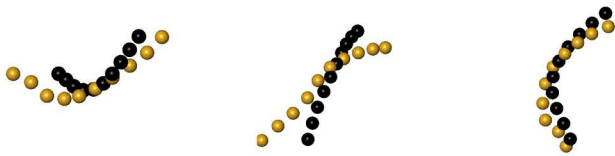
b) *Epipliopithecus*
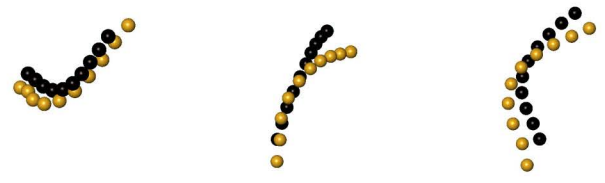
c) *Ekembo*

d) *Victoriapithecus*
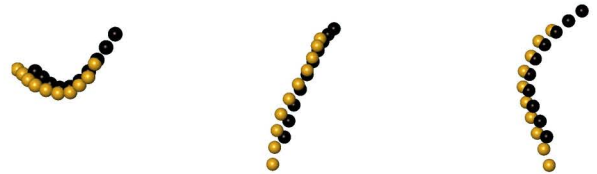
e) Crown platyrrhines
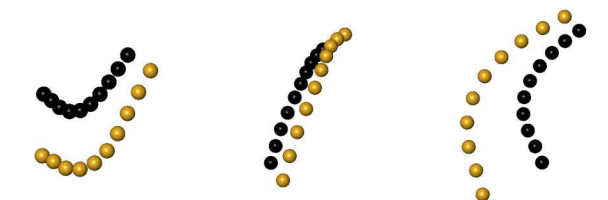
f) Crown catarrhines

g) Crown cercopithecoids

h) Crown hominoids

i) Crown hylobatids

j) Crown hominids

medial — posterior — anterior — lateral

superior — posterior — anterior — inferior

superior — lateral — medial — inferior

medial — posterior — anterior — lateral

superior — posterior — anterior — inferior

superior — lateral — medial — inferior
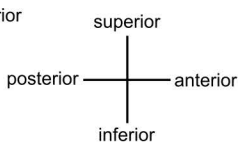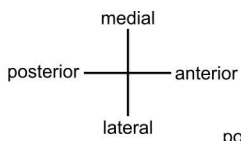
Table 1

Extant comparative sample used in this study based on μCT scans. Sample size and sex composition, institutional repository for the specimens, digital repository source, and voxel size range are indicated for each species. See SOM Table S1 for further details on the specimens included.

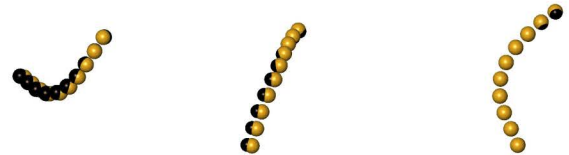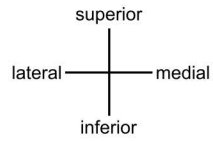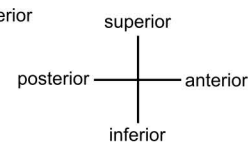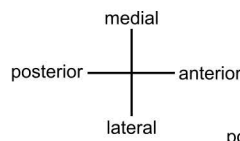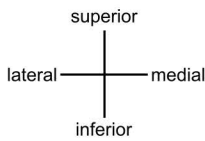| Taxon	Species	*n*	M	F	?	Repository	Source	Voxel size (μm)
Platyrrhini	*Alouatta palliata*	5	2	3	0	DUEA	MS	52–67
Platyrrhini	*Aotus griseimembra*	5	2	3	0	USNM	MS	34–38
Platyrrhini	*Ateles geoffroyi*	3	0	3	0	AMNH, MCZ	MS	62–63
Platyrrhini	*Cebus imitator*	3	0	3	0	MCZ	MS	80
Platyrrhini	*Chiropotes chiropotes*	3	1	2	0	USNM	MS	47–49
Platyrrhini	*Lagothrix lagotricha*	3	1	2	0	USNM	MS	58–60
Platyrrhini	*Mico argentatus*	3	2	1	0	MCZ	MS	40
Platyrrhini	*Pithecia monachus*	1	0	0	1	MCZ	MS	50
Platyrrhini	*Pithecia pithecia*	2	1	1	0	MCZ	MS	50
Platyrrhini	*Plecturocebus cupreus*	5	3	2	0	AMNH, MCZ	MS	47–51
Platyrrhini	*Saguinus fuscicollis*	1	0	1	0	AMNH	MS	27
Platyrrhini	*Saguinus midas*	2	2	0	0	MCZ	MS	40
Platyrrhini	*Saimiri sciureus*	3	1	1	1	MCZ	MS	47
Cercopithecidae	*Cercocebus torquatus*	2	2	0	0	AMNH	MS	90–120
Cercopithecidae	*Cercocebus galeritus*	1	1	0	0	AMNH, MCZ	MS	70
Cercopithecidae	*Cercopithecus mitis*	3	0	3	0	MCZ	MS	80
Cercopithecidae	*Chlorocebus pygerythrus*	3	1	2	0	SIU	MS	46–54
Cercopithecidae	*Colobus guereza*	3	1	2	0	AMNH	MS	66–73
Cercopithecidae	*Erythrocebus patas*	3	2	1	0	MCZ	MS	80
Cercopithecidae	*Lophocebus albigena*	3	1	2	0	MCZ	MS	90
Cercopithecidae	*Macaca fascicularis*	5	2	3	0	MCZ	MS	60–91
Cercopithecidae	*Mandrillus sphinx*	3	2	1	0	AMNH, MCZ	MS	75–126
Cercopithecidae	*Miopithecus talapoin*	3	3	0	0	MCZ	MS	50
Cercopithecidae	*Nasalis larvatus*	3	0	3	0	MCZ	MS	71

Cercopithecidae	*Papio anubis*	3	3	0	0	MCZ	MS	108–118
Cercopithecidae	*Piliocolobus badius*	3	2	1	0	MCZ	MS	80–90
Cercopithecidae	*Presbytis rubicunda*	3	1	2	0	MCZ	MS	80
Cercopithecidae	*Procolobus verus*	2	1	1	0	AMNH	MS	76–80
Cercopithecidae	*Semnopithecus entellus*	3	2	1	0	AMNH	MS	52–108
Cercopithecidae	*Simias concolor*	2	1	1	0	AMNH	MS	56
Cercopithecidae	*Theropithecus gelada*	3	2	1	0	AMNH	MS	84–120
Cercopithecidae	*Trachypithecus cristatus*	3	0	3	0	MCZ	MS	50
Hominidae	*Gorilla gorilla*	6	1	5	0	AMNH, MCZ	MS	106–131
Hominidae	*Pan paniscus*	5	1	3	1	AMNH, ICP, MCZ	MS, own data	66–116
Hominidae	*Pan troglodytes*	6	3	3	0	AMNH, ICP, MCZ	MS, own data	77–111
Hominidae	*Pongo* sp.	6	0	6	0	ICP, MCZ	MS, own data	77–125
Hylobatidae	*Hoolock hoolock*	3	1	2	0	AMNH	MS	52–84
Hylobatidae	*Hylobates agilis*	1	0	0	1	ICP	MS, own data	52
Hylobatidae	*Hylobates lar*	4	0	4	0	MCZ	MS	67
Hylobatidae	*Nomascus leucogenys*	1	1	0	0	AMNH	MS	105
Hylobatidae	*Symphalangus syndactylus*	2	0	2	0	AMNH	MS	62–79

Abbreviations: M = male; F = female; ? = unknown sex; AMNH = American Museum of Natural History, New York, USA; DUEA = Duke University, Evolutionary Anthropology, Durham, USA; ICP = acronym of the collections of the Institut Català de Paleontologia Miquel Crusafont, Sabadell, Spain; MCZ = Museum of Comparative Zoology, Harvard University, Cambridge, USA; MS = MorphoSource (https://www.morphosource.org); SIU = Southern Illinois University, Carbondale, USA; USNM = Smithsonian National Museum of Natural History, Washington, D.C., USA.

Table 2

Definition of the petrosal/tympanic landmarks used in this paper for aligning the specimens.

No.	Landmark	Definition
1	Porion	Most superior point on the margin of the external auditory meatus
2	Inferior external auditory meatus	Most inferior point on the margin of the external auditory meatus
3	Posterior external auditory meatus	Most posterior point on the margin of the external auditory meatus
4	Posterior internal auditory meatus	Most posterior point on the margin of the internal auditory meatus
5	Anterior internal auditory meatus	Most anterior point on the margin of the internal auditory meatus
6	Medial anterior pyramidal ridge	Most medial point where anterior pyramidal ridge starts running laterally above the fossa for the semilunar ganglion
7	Intersection ridge-groove	Point of intersection between the laterally running anterior pyramidal ridge and the groove of the greater petrosal nerve
8	Greater petrosal nerve hiatus	Most superior, anterior point on the margin of the hiatus for the greater petrosal nerve
9	Stylomastoid foramen	Center of the stylomastoid foramen

Table 3

Descriptive statistics of the variables describing the orientation, proportions and course of the carotid canal in the main extant anthropoid clades. See SOM Table S2 for the individual values of extant anthropoid specimens.

Clade	n	2DYZA			2DXYA			$L/V^{(1/3)}$			bgPC1			bgPC2		
		Mean	SD	Range	Mean	SD	Range	Mean	SD	Range	Mean	SD	Range	Mean	SD	Range
Platyrrhini	39	64.06	7.33	50.66–79.36	31.92	7.57	8.25–44.26	3.68	0.39	2.90–4.42	-0.36	0.11	0.50–0.07	-0.01	0.11	-0.26–0.17
Cercopithecidae	54	69.71	7.42	57.2–85	16.69	10	-3.54–33.87	2.86	0.42	1.40–3.87	0.17	0.08	-0.11–0.34	-0.04	0.09	-0.29–0.14
Hominidae	23	54.90	7.83	37.27–69.11	13.74	7.38	-0.82–27.78	3.23	0.31	2.57–3.82	0.12	0.08	-0.10–0.20	0.12	0.05	-0.01–0.20
Hylobatidae	11	54.51	12.39	38.27–78.27	10.27	7.44	1.00–23.27	2.68	0.47	1.97–3.37	0.18	0.08	0.06–0.32	-0.04	0.10	-0.25–0.12

Abbreviations: 2DYZA = 2D angle in the YZ plane (canal superior orientation; in degrees); 2DXYA = 2D angle in the XY plane (canal medial orientation; in degrees); L = length (in mm); V = volume (in mm^3); bgPC = between-group principal component.

Table 4

Variables describing the orientation, proportions and course of the carotid canal in the fossil specimens.

Species	Catalog No.	2DYZA	2DXYA	L/V$^{(1/3)}$	bgPC1	bgPC2
Ekembo heseloni	KNM-RU 2036al	53.58	34.73	3.12	-0.02	-0.03
Epipliopithecus vindobonensis	NHMW 1970/1397/0003	53.59	27.62	3.05	-0.08	-0.06
Pliobates cataloniae	IPS58443.1	35.58	16.86	3.58	-0.03	0.05
Victoriapithecus macinessi	KNM-MB 29100	66.73	10.36	3.25	-0.02	-0.04

Abbreviations: 2DYZA = 2D angle in the YZ plane (canal superior orientation; in degrees); 2DXYA = 2D angle in the XY plane (canal medial orientation; in degrees); L = length (in mm); V = volume (in mm^3); bgPC = between-group principal component.

Table 5

Z-score analysis of the three variables describing the orientation, proportions and course of the carotid canal in the fossil specimens and compared to the variation expressed by the main extant anthropoid clades.[a]

Variable and species	Catalog No.	Platyrrhini	Cercopithecidae	Hominidae	Hylobatidae
2DYZA					
Ekembo heseloni	KNM-RU 2036al	-1.43	**-2.17**	-0.17	-0.08
Epipliopithecus vindobonensis	NHMW 1970/1397/0003	-1.43	**-2.17**	-0.17	-0.07
Pliobates cataloniae	IPS58443.1	**-3.88**	**-4.60**	**-2.46**	-1.52
Victoriapithecus macinnesi	KNM-MB 29100	0.36	-0.40	1.51	0.98
2DXYA					
Ekembo heseloni	KNM-RU 2036al	0.37	1.80	**2.84**	**3.29**
Epipliopithecus vindobonensis	NHMW 1970/1397/0003	-0.56	1.09	1.88	**2.33**
Pliobates cataloniae	IPS58443.1	**-1.99**	0.02	0.42	0.89
Victoriapithecus macinnesi	KNM-MB 29100	**-2.85**	-0.63	-0.46	-0.02
L/V$^{(1/3)}$					
Ekembo heseloni	KNM-RU 2036al	-1.46	0.61	-0.36	0.93
Epipliopithecus vindobonensis	NHMW 1970/1397/0003	-1.64	0.44	-0.58	0.78
Pliobates cataloniae	IPS58443.1	-0.27	1.69	1.09	1.89
Victoriapithecus macinnesi	KNM-MB 29100	-1.13	0.91	0.04	1.20
bgPC1					
Ekembo heseloni	KNM-RU 2036al	**3.23**	**-2.30**	-1.78	**-2.39**
Epipliopithecus vindobonensis	NHMW 1970/1397/0003	**2.70**	**-2.97**	**-2.50**	**-3.08**
Pliobates cataloniae	IPS58443.1	**3.14**	**-2.41**	-1.90	**-2.51**
Victoriapithecus macinnesi	KNM-MB 29100	**3.19**	**-2.35**	-1.83	**-2.45**
bgPC2					
Ekembo heseloni	KNM-RU 2036al	-0.25	0.02	**-3.16**	0.04
Epipliopithecus vindobonensis	NHMW 1970/1397/0003	-0.51	-0.31	**-3.78**	-0.27
Pliobates cataloniae	IPS58443.1	0.48	0.93	-1.47	0.87
Victoriapithecus macinnesi	KNM-MB 29100	-0.25	0.02	**-3.17**	0.03

Abbreviations: 2DYZA = 2D angle in the YZ plane (canal superior orientation; in degrees);

2DXYA = 2D angle in the XY plane (canal medial orientation; in degrees); L = length (in mm);

V = volume (in mm^3); bgPC = between-group principal component.

[a] Significant z-scores at $p < 0.05$ are bolded.

Table 6

Phylogenetic generalized least-squares (PGLS) allometric regressions between carotid canal size variables (L, $V^{1/3}$ or CS) or between carotid canal size and BM, together with PGLS bivariate regressions between carotid canal shape (as represented by the canal robusticity index or bgPCs) vs. log-transformed carotid canal size or BM.

Regression	p[a]	R^2	Slope	Slope 95% CI
ln L vs. ln $V^{1/3}$	<0.001	0.81	0.86	0.73, 0.99
ln L vs. ln $V^{1/3}$ [b]	<0.001	0.81	0.95	0.81, 1.10
L/$V^{1/3}$ vs. ln CS	>0.05	-0.02	0.11	–0.34, 0.57
ln L vs. ln CS	<0.001	0.99	1.04	1.02, 1.06
ln $V^{1/3}$ vs. ln CS	<0.001	0.81	0.99	0.84, 1.13
ln L vs. ln BM	<0.001	0.68	0.25	0.20, 0.31
ln $V^{1/3}$ vs. ln BM	<0.001	0.90	0.30	0.27, 0.34
ln CS vs. ln BM	<0.001	0.69	0.25	0.19, 0.30
L/$V^{1/3}$ vs. ln BM	<0.01	0.14	-0.17	–0.29, –0.05
bgPC1 vs. ln CS	>0.05	0.01	0.12	–0.07, 0.31
bgPC1 vs. ln $V^{1/3}$	<0.01	0.19	0.26	0.10, 0.41
bgPC1 vs. ln BM	<0.001	0.25	0.10	0.05, 0.15
bgPC2 vs. ln CS	<0.001	0.58	0.21	0.16, 0.27
bgPC2 vs. ln $V^{1/3}$	<0.001	0.46	0.17	0.11, 0.23
bgPC2 vs. ln BM	<0.001	0.35	0.05	0.04, 0.08

Abbreviations: L = carotid canal length (mm); $V^{1/3}$ = carotid canal volume cube root (mm); L/$V^{1/3}$ = shape index of canal robusticity; CS = carotid canal centroid size (mm); BM = body mass (g); bgPC = between-group principal component (representing carotid canal course).

[a] Regressions are significant when $p < 0.05$.

[b] For ln L vs. ln $V^{1/3}$, a major axis regression was also computed to test whether the two variables are isometric when deviation from the best-fit line is minimized simultaneously for both variables (instead of only the dependent variable, in this case ln L). Our results show that, unlike for the PGLS regression (which displays slight negative allometry), isometry cannot be discounted for the major axis regression.

Table 7

Number (*n*) and percentages (%) of correctly and incorrectly classified individuals obtained by the between-group principal components analysis after cross-validation. In total, 98 out of 127 (77.2%) individuals were correctly classified (in bold).

	Platyrrhini	Cercopithecidae	Hominidae	Hylobatidae
Platyrrhini	**36 (92.3%)**	0 (0%)	0 (0%)	3 (7.7%)
Cercopithecidae	1 (1.9%)	**34 (63.0%)**	9 (16.7%)	10 (18.5%)
Hominidae	0 (0%)	2 (8.7%)	**21 (91.3%)**	0 (0.0%)
Hylobatidae	0 (0%)	3 (27.3%)	1 (9.1%)	**7 (63.6%)**

Table 8

Posterior probabilities of group membership based on the between-group principal component scores of fossil specimens.[a]

Species	Catalog No.	Platyrrhini	Cercopithecidae	Hominidae	Hylobatidae
Ekembo heseloni	KNM-RU 2036al	<0.001	**0.098**	0.059	0.087
Epipliopithecus vindobonensis	NHMW 1970/1397/0003	<0.001	**0.018**	0.009	0.016
Pliobates cataloniae	IPS58443.1	<0.001	0.064	**0.169**	0.056
Victoriapithecus macinessi	KNM-MB 29100	<0.001	**0.089**	0.054	0.079

[a] Each value corresponds to the probability of having the given score if the specimen was a member of the group considered, not the likelihood of group membership in each of the a priori defined groups given a particular score (the greater the number, the higher the probability). For each specimen the highest probability is bolded.